

3. MATERIALS PROCESSING TECHNOLOGIES

A. Oxidative Stabilization of PAN Fiber Precursor

Principal Investigator: Felix L. Paulauskas

Oak Ridge National Laboratory

Oak Ridge, TN 37831-8048

(865) 576-3785; fax: (865) 574-8257; e-mail: paulauskasfl@ornl.gov

Project Manager, Composites: C. David Warren

Oak Ridge National Laboratory

P.O. Box 2008, Oak Ridge, TN 37831-6065

(865) 574-9693; fax: (865) 576-4963; e-mail: warrencd@ornl.gov

Technology Development Area Specialist: Sidney Diamond

(202) 586-8032; fax (202) 586-2476; e-mail: sid.diamond@hq.doe.gov

Field Technical Manager: Philip S. Sklad

(865) 574-5069; fax:(865) 576-4963; e-mail: skladsps@ornl.gov

Participants

Terry L. White and Kenneth D. Yarborough, Oak Ridge National Laboratory

Professor Joseph Spruiell, University of Tennessee

Daniel Sherman, Atmospheric Glow Technologies

Contractor: Oak Ridge National Laboratory

Contract No.: DE-AC05-00OR22725

Objectives

- Develop an improved technique for oxidizing carbon fiber precursor with increased line speed, reduced carbon fiber cost, and reduced equipment footprint.
- Verify that produced fiber properties satisfy automotive and heavy vehicle manufacturers' requirements.
- Conduct a preliminary evaluation of the cost impact of the new oxidation technique.

Approach

- Develop a plasma process for oxidation in an atmospheric-pressure plasma reactor.
- Develop fiber handling protocols for continuous processing.
- Conduct parametric studies to correlate processing parameters and fiber properties.
- Characterize fibers to confirm that they satisfy program requirements.

Accomplishments

- Demonstrated the ability to oxidize fiber in atmospheric-pressure plasma in stages equivalent to those used in conventional oxidation furnaces.
- Identified key process parameters and critical operating range and modified the reactor to achieve stable operation in the required parametric space.

- Identified the preferred range of feed gas compositions.
- Improved dielectric properties monitoring technology and presented a conference paper on that topic.

Future Direction

- Continue refining the reactor design and processing protocols to achieve rapid, single-stage fiber oxidation.
 - Develop “pre-stabilization” technique.
 - Develop continuous processing protocols.
 - Conduct parametric studies and fiber characterization to better understand process effects and the processing window and to quantify fiber properties.
 - Conduct rate-effect studies and update cost analysis.
-

Introduction

The purpose of this project is to investigate and develop a plasma processing technique to rapidly and inexpensively oxidize a polyacrylonitrile (PAN) precursor. Oxidative stabilization is a slow thermal process that typically consumes 70% or more of the processing time in a conventional carbon fiber conversion line. A rapid oxidation process could dramatically increase the conversion line throughput and appreciably lower the fiber cost. A related project has already demonstrated the potential for greatly increasing line speed in the carbonization and graphitization stages, but the oxidation time must be greatly reduced to fully exploit faster carbonization and graphitization. This project intends to develop a plasma oxidation module that integrates with other advanced fiber processing modules to produce inexpensive carbon fiber with properties suitable for use by the automotive industry. Critical technical criteria include (1) 25 Msi tensile modulus, 250 ksi ultimate strength, and 1.0% ultimate strain in the finished fiber; (2) acceptably uniform properties over the length of the fiber tow; (3) repeatable and controllable processing; (4) and significant unit cost reduction compared with conventional processing.

Project Deliverable

At the end of this project, we will have demonstrated satisfactory fiber oxidation in a multiple-tow plasma oxidation module operating at line speed exceeding that typical of conventional carbon fiber conversion lines.

Technical Approach

We are investigating PAN precursor fiber oxidation by “direct exposure” in a nonequilibrium, nonthermal plasma at atmospheric pressure, with the fiber transported through the plasma. Plasma processing is believed to enhance oxygen diffusion and chemistry in the PAN oxidation process. Atmospheric-pressure plasma provides better control over the thermal environment and reaction rates than does evacuated plasma, in addition to eliminating the sealing problems accompanying evacuated plasma processing. Various fiber characterization tools and instruments are used to conduct parametric studies and physical, mechanical, and morphological evaluations of the fibers to optimize the process. An evacuated plasma reactor is useful for bench-scale studies, because it allows a greater degree of manipulation and control over reactive species and related parameters. Early in the project, processing tests were conducted in an evacuated plasma reactor, and that same reactor is now used for conducting the bench-scale parametric studies.

Atmospheric-Pressure Plasma Processing Results

Exposure in plasma at or near atmospheric pressure provides superior thermal control because the gas flow should convectively heat or cool the fibers. This is deemed particularly important to avoid fiber melting from the exothermic reactions associated with the PAN cross-linking that occurs during stabilization. However, the mean free path of the chemically reactive species is shorter by orders of magnitude than it is in an evacuated environment, and this makes it very difficult to find a combination

of process parameters that will oxidize the fibers with acceptable residence time.

Conventional PAN oxidation is typically accomplished in three or four thermal stages (stages can be physically separate furnaces or zones in a single physical furnace) in air, at temperatures increasing from about 200 to 250°C. In FY 2004, the researchers demonstrated the ability to reproduce the oxidation advancement in each of the conventional furnaces two, three, and four. The virgin PAN is chemically fragile; hence we have not yet discovered a satisfactory nonthermal processing protocol that reproduces the oxidation advancement in the first conventional furnace. Subsequent experiments have demonstrated the ability to advance the oxidation from the beginning of furnace two through the exit of furnace three in a single, uninterrupted process. These processing results are schematically illustrated in Figure 1.

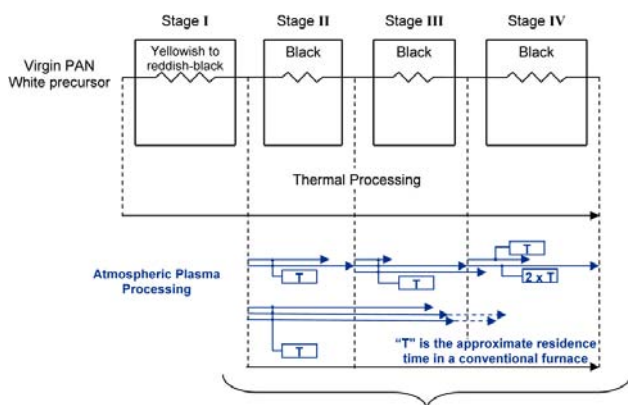


Figure 1. Schematic of conventional thermal oxidation process and progress in plasma oxidation process.

A potentially very important discovery was that the cores of plasma-oxidized fibers are more chemically stable than those of conventionally processed fibers. Figure 2 illustrates the advancement of oxidation and stabilization through a filament cross-section. Most of the fiber must be oxidized, as represented by the outer region, before it can withstand carbonization. In thermal oxidation, the outer stabilized and oxidized region grows inward slowly, purely by diffusion. However, in plasma oxidation, we have observed that oxidation over the filament cross-section is much more uniform; and the entire fiber becomes highly oxidized at a lower fiber density (fiber density is normally used as an indicator of

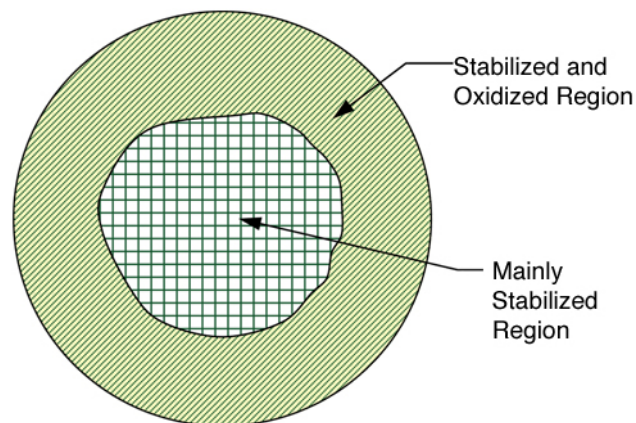


Figure 2. Illustration of advancing oxidation and stabilization through filament cross-section.

degree of oxidation advancement). This suggests that plasma oxidation may allow onset of carbonization at a lower fiber density, a thesis that will be experimentally tested in future work. If carbonization can indeed commence at a lower fiber density, this could significantly reduce the residence time required for oxidation.

The researchers have made good progress toward identifying the parameters that most affect the oxidation rate and optimizing those parameters within the reactor. For patent protection and export control reasons, the detailed results are not published, but they are periodically disclosed to the relevant program managers in oral briefings.

Feed Gas Composition

The researchers investigated the effects of plasma oxidation with various gas compositions. It was confirmed that the chemistry can be quite sensitive to feed gas composition, as illustrated in Figure 3. A wide range of feed gas compositions were investigated and the results recorded. Specific compositions and processing parameters are not published for patent protection and export control reasons.

Instrumentation

During this reporting period, the researchers continued developing techniques and hardware for measuring the fiber dielectric properties over a selected range of oxidation processing conditions. A dielectric measurement system, shown schematically in Figure 4, was validated. Several temperature

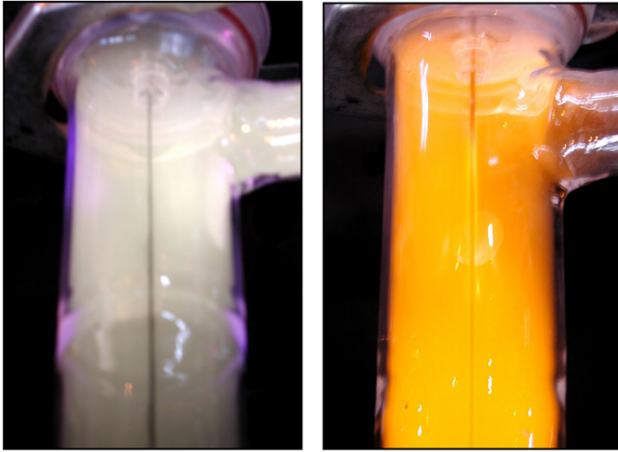


Figure 3. Plasma with two different feed gas compositions in evacuated plasma reactor.

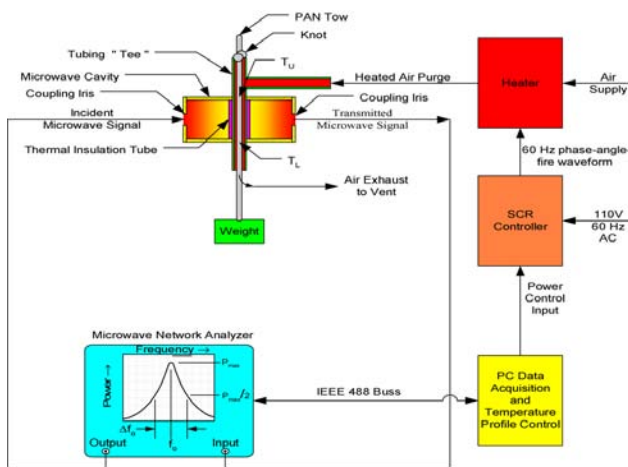


Figure 4. Dielectric measurement system schematic.

control problems were identified and corrected by adjusting control and operational parameters, modifying hardware, and changing the PAN cross-section in the instrument chamber. A large number of runs were conducted with PAN partially oxidized to differing degrees. The real and imaginary parts of the dielectric constant correlated well with the degree of PAN oxidation. A paper on this topic was presented at the 2004 SAMPE Symposium and Exposition in Long Beach CA.

The researchers began creating a dielectric properties database for 3-k and 80-k PAN fiber tows that were partially oxidized in varying degrees by conventional means. Plasma-oxidized fiber properties can later be compared against this database as a selector for fiber specimens that will be further characterized by more time-consuming spectroscopy techniques.

The researchers need a rapid turnaround technique for indicating oxidation trends, to quickly assess whether various parametric processing trials have successfully advanced the oxidation. Density measurements are frequently used by fiber manufacturers. In this project, dielectric measurement equipment and techniques have been successfully developed and validated, and morphology measurements are also used to characterize the fibers. However, density, dielectric, and morphology measurements all have turnaround times of hours to days because of measurement duration, instrument cost and location, required operator skill, and/or instrument time-sharing. The fiber changes color, starting from white and successively darkening until it turns completely black after it is about 10–20% oxidized. Therefore, color is a reasonable progress indicator in early oxidation, but another technique is needed for the remainder of oxidation.

The researchers investigated dc electrical resistance measurement as an oxidation progress indicator. The very high tow resistance ($10^{12} - 10^{15}$ ohms) is beyond the capability of most resistance meters and can be accurately measured only under exceedingly well-controlled environmental conditions. A high-resistance meter was purchased and tested. The PAN fiber must present the most conductive path between measurement terminals to achieve accurate resistance measurement. Since moisture, and even air, can provide a conductive “short,” the researchers concluded that dc resistance measurements are too unreliable, even with meters rated for ultra-high resistance. The researchers are still searching for a good, inexpensive, rapid turnaround technique for monitoring the relative oxidation progress.

Economics

During FY 2004, Kline and Company completed a cost study of DOE’s entire carbon fiber development program, estimating profitable selling prices for baseline technology and if various technologies under development were implemented. Kline’s estimates generally indicated that advanced oxidation techniques should reduce fiber selling price by about 6–8%. These estimates, however, were based on a line speed comparable to that of conventional conversion lines. Rough calculations suggest that if we can achieve much higher line speeds, the savings could increase dramatically. We have not discovered any inherent physics limits that would prevent us

from achieving a large increase in conversion line speed using plasma oxidation and microwave-assisted plasma carbonization.

Education

The materials characterization has been conducted in partnership with the University of Tennessee's (UT's) materials science department. Two UT graduate students were engaged to provide characterization support to the project.

Partners

ORNL gratefully acknowledges contributions to this project by Fortafil and Hexcel. Both have generously provided raw materials and offered technical consultation. An updated materials transfer agreement was executed with Hexcel during this reporting period. Additionally, technical and programmatic consultation has been provided by the Automotive Composites Consortium and by Delphi Corporation.

Conclusions

The development of plasma-based oxidation technology has achieved a major milestone by dem-

onstrating the feasibility of plasma processing to oxidize PAN precursor fibers. Preliminary data suggest that the plasma oxidation process may allow earlier onset of carbonization, thus reducing oxidation residence time. Understanding of the parametric processability space has grown substantially during this period. Preliminary economics studies support the value of research in advanced oxidation. The researchers expect to demonstrate continuous plasma processing, and continue growing our understanding of the plasma oxidation process and its benefits, in FY 2005.

Presentations

F. L. Paulauskas and T. L. White, "Temperature-Dependent Dielectric Measurements of Polyacrylonitrile Fibers during Air Oxidation," 49th International SAMPE Symposium 2004, Long Beach, CA. May 16–20, 2004. Published in the conference proceedings, 2004.

B. Wrought Magnesium Alloy/Process Development

Principal Investigator: J. A. Horton

Oak Ridge National Laboratory

P.O. Box 2008, Oak Ridge, TN 37831-6115

(865) 74-5575; fax: (865) 574-825; hortonja@ornl.gov

Principal Investigator: S. R. Agnew

University of Virginia

116 Engineer's Way

P.O. Box 400745, Charlottesville, VA 22904-4745

Technology Development Area Specialist: Sidney Diamond

(202) 586-8032; fax: (202) 586-1600; e-mail: sid.diamond@ee.doe.gov

Field Technical Manager: Philip S. Sklad

(865) 574-5069; fax: (865) 576-4963; e-mail: skladps@ornl.gov

Contractor: Oak Ridge National Laboratory

Contract No.: DE-AC05-00OR22725

Objectives

- Develop wrought magnesium alloys with better formability than current magnesium alloys.
- Investigate new processing techniques for cost reduction and formability improvement.
- Contribute to basic understanding of deformation, processing, and alloy behavior for this lightweight metal.

Approach

- Explore new processing schemes for magnesium alloy sheets.
- Evaluate the practical formability of new alloys and after new processes.
- Determine deformation mechanisms using experimentation and simulation.

Accomplishments

- Demonstrated feasibility of infrared sheet processing at a commercial facility, Manufacturing Sciences, Inc.
- Designed warm formability testing tool based upon the "OSU test."
- Experimentally validated the dislocation-based mechanism hypotheses developed through simulation.
- Collected data to determine if various dislocation-based mechanisms have distinct grain-size dependence.
- Completed assessment of texture evolution during equal channel angular extrusion.

Future Direction

- Interact with an industrial partner to advance commercialization of infrared processing for cost reductions.
- Define further correlations of microstructure, mechanisms, and anisotropy.

- Further explore superplastic-type behavior observed at warm forming temperatures.
- Investigate fundamental parameters affecting castability of the more creep-resistant alloys.

Introduction

The world market for magnesium has changed substantially in recent years with the emergence of China as the leading producer (~50% of the market.) For instance, some western competitors have been driven out of business (e.g., Noranda in Canada) or have uncertain futures (e.g., AMC in Australia). It is still unclear what the final outcome will be, since at least one major western supplier (Norsk Hydro) has formed an alliance with a Chinese partner. Magnesium sheet manufacturers face a number of technical issues that we continue to research:

- Rolling magnesium to thin-gage sheet currently leads to expensive solutions.
- Obtaining an excellent surface finish is difficult.
- Corrosion performance is poor vis-a-vis die-cast alloys.
- Sheet formability is limited at low temperatures.

During FY 2003, in addition to focusing on the sheet formability issues, we began addressing the concerns associated with the cost of sheet products.

Demonstration of Infrared Processing at A Commercial Rolling Facility

After lab studies of the relevant infrared parameters, microstructures, and mechanical properties involved with infrared processing of sheet magnesium, a demonstration was performed at Manufacturing Sciences under the direction of Tom Muth. This commercial rolling mill facility has a 3 × 8 ft bank of infrared lamps at 12 W/cm² installed on one side of a reversing mill (Figure 1). Starting material for this demonstration was commercial sheets of 6-mm-thick AZ31 tooling plate. Initial heatup required 5 min; subsequent heatups with thinner sheet required less time until the last pass required approximately 2 min. Newer designs of the infrared bank have an even higher output, promising even shorter anneal times.

Sets of rolling sequences were performed aiming at 15%, 20%, and 40% rolling reductions for each pass until 1-mm thickness was obtained. A fi-



Figure 1. Commercial rolling mill facility has a 3 × 8 ft bank of infrared lamps at 12 W/cm² installed on one side of a reversing mill.

nal roll on a 6-mm plate was performed with as much reduction as we dared. Desired temperatures were 400°C and 500°C. However, 500°C could not be reached because of the large airflow. Specimens were collected at several points in the rolling sequence. Table 1 lists the as-rolled mechanical properties for five test runs at various points during the rolling. The amount of cold work saturated after few passes. However, the tensile strengths and ductilities indicate that the magnesium was essentially cold-rolled. Further experiments are under way to attempt to study actual rolling temperature effects on texture and properties.

Figure 2 shows that the microstructure in the near-surface regions was similar to that of the cen-

Table 1. As-rolled mechanical property data after infrared processing

T (°C)	Average reduction (%)	Thickness (mm)	Passes	UTS (MPa)	Elongation (%)
400	16.5	2.1	6	275	6
		1.3	9	285	5
		1.0	10	307	4
400	23	1.5	5	298	6
		1.0	7	404	7
~425	44	1.1	3	363	3
~425	66	2.1	1	265	5

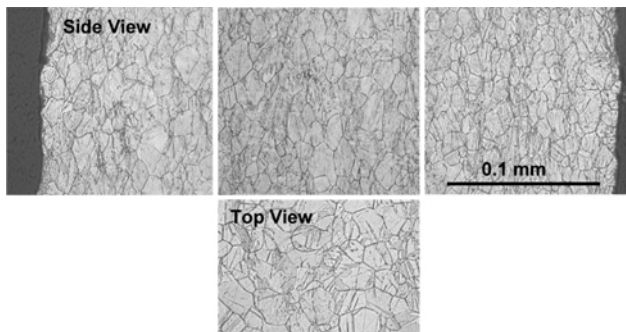


Figure 2. Side and top views of the microstructure of 1mm thick sheets after the 10th pass at average of 16.5% reduction showing that the near surface regions were similar to the center.

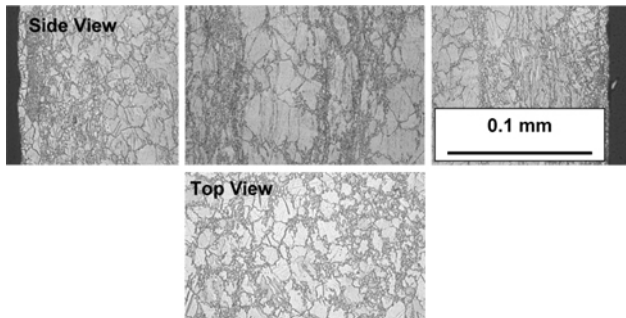


Figure 3. Side and top views of the microstructure sheets after a single pass of 66% reduction showing evidence of dynamic recrystallization in the form of fine grain necklaces.

ter. The largest reduction used, 66%, resulted in some dynamic recrystallization, as shown in Figure 3. Such an approach could be used to develop a very fine-grained structure appropriate for superplastic forming, as an example. In addition to microstructure, we examined the texture, since it is so significant for determining the properties of magnesium. The (0002) pole figure from the as-received 6-

mm tooling plate was little changed by the infrared rolling.

These results were presented at the Magnesium 2004 symposium at the TMS annual meeting and generated much interest. A member of the audience raised the concern that such large reductions could introduce microcracks or other defects during this processing, resulting in the low ductilities shown in Table 1. Subsequent annealing studies for 2 hours at 185°C and 345°C resulted in much higher ductilities, suggesting that normal commercial wrought properties, or better, can be obtained (see Table 2).

Table 2. Mechanical property data after 2-hour anneals

Anneal T (°C)	Yield (MPa)	UTS (MPa)	Elongation (%)
As-rolled	262±57	312±49	5±2
185	185±11	269±6	18±2
345	141±14	247±6	24±2

Design and Implementation of a Warm Formability Testing Apparatus

Throughout our research project, we have been continually pursuing the possibility of forming magnesium sheet metal at lower temperatures. Traditional wisdom states that the forming temperatures should be in the range of 250°C or higher. One problem is that there really is no standardized testing methodology for warm forming. In the past, we have used a high-temperature cylindrical cup drawing apparatus at Oak Ridge National Laboratory as an indicator of formability; and we have been able to make qualitative comparisons between alloys. However, there are a couple of problems with this ap-

proach: (1) Since our target applications are vehicles, the most important forming operations tend to be primarily stretching, as opposed to drawing. (2) The results of the cup drawing test are heavily influenced by thermal gradients. In our case, the die is heated, but the punch is not. While this actually leads to enhanced practical formability, it is not the best way to assess the intrinsic formability of the material at a given temperature and strain rate.

We studied the literature and found a new test developed at Ohio State University (the OSU test) that actually deforms the sheet metal in a condition very close to plane strain tension. This is significant, since studies of technological forming failures have indicated 80% of stamping failures are under conditions of plane strain. This is also the division between the drawing and stretching halves of the forming limit diagram (FLD); it yields a result known as FLD_0 , which is the lowest point on the FLD. This test requires a relatively small die set-up and thus can fit within one of the furnaces mounted on mechanical testing frames at the University of Virginia (Figure 4). A few trial runs on copper and aluminum alloy sheets have been performed at ambient temperatures. Once a protocol has been developed, warm formability tests on aluminum and magnesium alloys will be performed. These may be conventional alloy sheets, sheets subjected to novel processing schemes, or experimental alloys.

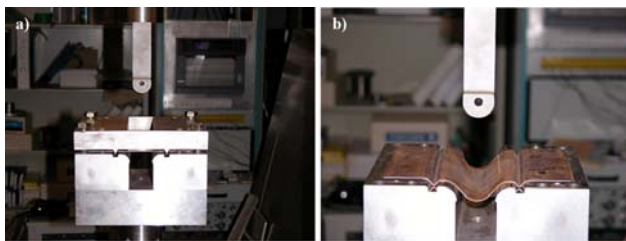


Figure 4. Warm formability testing apparatus based upon “the OSU test” shown (a) prior to deformation, as the metal is being clamped into the die, and (b) after deformation.

Validation of Anisotropy and Simulation Approach to Mechanism Determination

It is of interest to determine the deformation mechanisms that control the deformation behavior of wrought magnesium. For instance, if particular mechanisms can be determined to be responsible for the cold-formability problems or the excellent formability at elevated temperatures, improvements may

be made through targeted alloy or microstructure design. Our approach has been to probe the deformation mechanisms with the help of computer simulations based on polycrystal plasticity theory. Information about the material’s structure (i.e., crystallographic texture) and deformation mechanisms (solved for iteratively) serves as input, and the mechanical behavior and texture evolution are outputs. Experimentally, the initial texture, the mechanical response, including anisotropy, and the final texture are measured. When the simulations predict the observed behavior, it is an indication that the deformation mechanisms used as inputs are reflective of the material’s mechanisms.

Last year it was demonstrated that alloy AZ31B sheet exhibits a strong correlation between the sharp increase in tensile ductility (and formability in general) at mildly elevated temperatures and a sharp decrease in anisotropy (Figure 5). Through the approach outlined, it was suggested that this strong decrease in anisotropy is associated with the activation of another deformation mechanism at elevated temperatures, pyramidal $\langle c+a \rangle$ slip. Of all the slip mechanisms known to operate within magnesium, this was the only one for which the simulations predicted the observed lowering of anisotropy. Provided the intrinsic assumptions of polycrystal plasticity are correct, this would represent a significant finding.

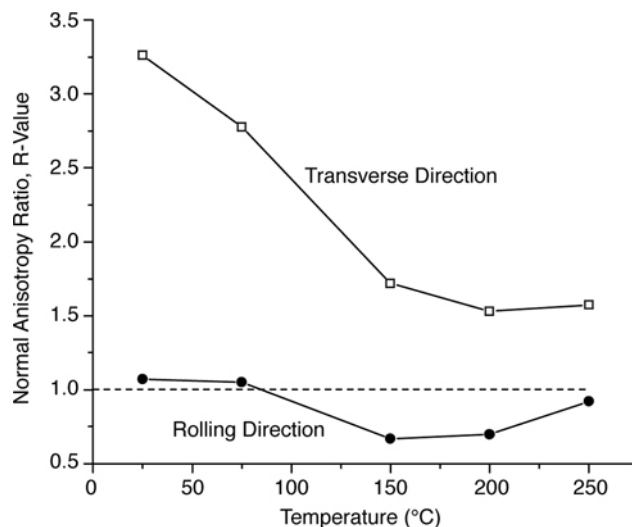


Figure 5. The r-value measurements over a range of temperatures show that the r-value drops strongly in all directions as the temperature is raised. This behavior has been linked to an increase in the activity of pyramidal $\langle c+a \rangle$ slip as the temperature is raised.

This year, efforts have been focused on demonstrating that the predictions of the approach are grounded in reality. Transmission electron microscope (TEM) dislocation analysis was used to examine deformed samples for evidence of mechanisms predicted to be operational by the modeling approach. As an initial step, samples deformed at room temperature were examined for evidence of non-basal $\langle a \rangle$ slip. The simulations suggested that up to 80% of strain is accommodated by non-basal slip. This is in stark contrast with magnesium single-crystal observations of the 1950s and 1960s, which showed no evidence of non-basal slip below $\sim 180^\circ\text{C}$, even under constraint. The TEM study did show evidence of extensive non-basal $\langle a \rangle$ dislocation slip (Figure 6), and a preliminary report was published in the *Proceedings of the Magnesium Technology 2004 Symposium of the TMS Annual Meeting*. A full journal paper in the *International Journal of Plasticity* is in-press.

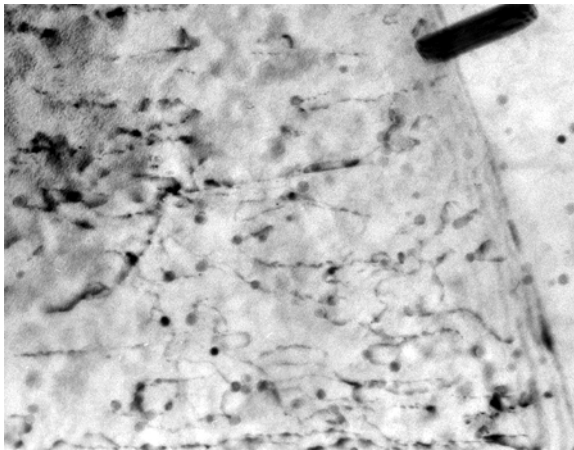


Figure 6. TEM image of magnesium alloy AZ31B deformed in tension shows curved dislocations when viewing from a basal plane edge-on perspective. Thus the dislocations are gliding on non-basal planes. A complete Burgers vector analysis shows the majority of dislocations to have $b = \frac{1}{3}[11\bar{2}0]$ or $[a3]$.

The same approach is being applied to determine (1) whether non-basal slip is strongly controlled by grain size and (2) whether our hypothesis that high-temperature formability is controlled by $\langle c+a \rangle$ slip is correct. Both of these findings would have significant practical implications, since processing can strongly affect the microstructure of magnesium (see following discussion), and secondary slip can be heavily influenced by alloying additions.

Samples of alloy AZ31 sheet with different linear intercept grain sizes (14–220 μm) have been produced through annealing for different times (1 h–1 week) and temperatures (345–525 $^\circ\text{C}$). To date, the grain size has been assessed and tensile tests along the rolling (RD) and transverse (TD) directions have been performed, since these were previously shown to exhibit distinct behaviors connected with varying ratios of basal : non-basal dislocation slip (Figure 7a). Plotting the results in the conventional Hall-Petch fashion (Figure 7b) reveals a grain size dependence of this alloy’s yield strength similar to that published previously.^{1,2}

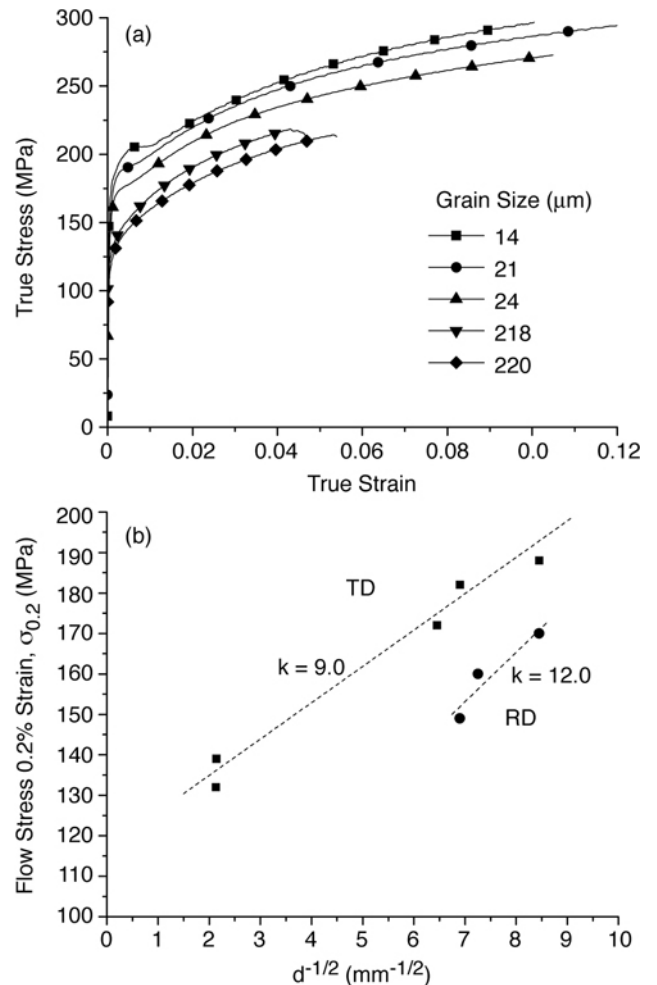


Figure 7. Grain size dependence of the (top) flow curves for transverse direction samples and (bottom) the yield stresses of both transverse and rolling direction samples of magnesium alloy AZ31 sheet.

More interesting are the differences in the anisotropy that are exhibited by samples of different

grain sizes (Figure 8). The as-received (not annealed) samples exhibit the lowest anisotropy. Annealing and grain growth actually appear to enhance the anisotropy, contrary to popular opinion. If the r-values are measured at a strain of 11%, as we have done previously, there appears to be only a slight change with annealing.

A special extensometer has been obtained that can measure the Poisson strain along the sample's width direction in-situ. The r-value evolution can be determined

$$r = \varepsilon_w / \varepsilon_t = -\varepsilon_w / (\varepsilon_l + \varepsilon_w)$$

by virtue of the incompressible nature of metal plasticity ($\varepsilon_w + \varepsilon_t + \varepsilon_l = 0$), where ε_w , ε_t , and ε_l are the strains along the sample's width, thickness and length directions. This new tool shows the evolution of anisotropy is strikingly different between the samples of different grain sizes (Figure 8).

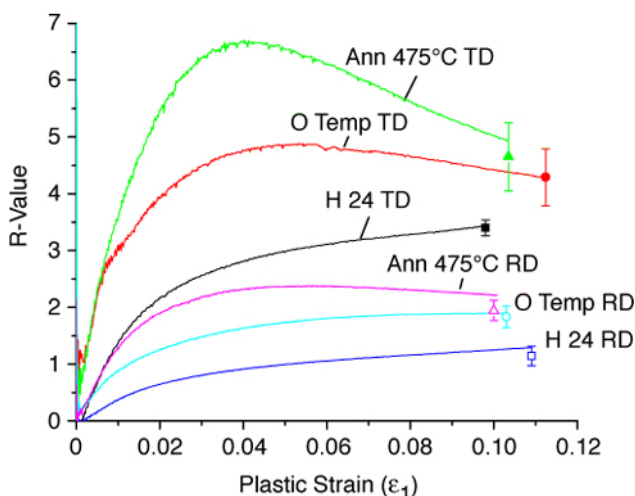


Figure 8. Evolution of the anisotropy (r-value) with strain for samples of different grain sizes (H24 temper $\sim 9 \mu\text{m}$, O temper $\sim 14 \mu\text{m}$, and annealed at $475^\circ\text{C} > 30 \mu\text{m}$).

It was anticipated that larger grain samples might exhibit less non-basal slip and therefore lower r-values (using modeling arguments discussed earlier.) However, the initial results show that all of the larger grain samples have higher r-values. This fact may not be linked to mechanistic changes, since the higher overall anisotropy may be connected with a change in the texture during annealing; so we are now measuring the textures of samples in addition to their grain size. The final results will be important

input for microstructure design of wrought magnesium.

Texture Evolution during Equal Channel Angular Processing

This project focused on wrought magnesium began with an investigation of the potential of equal channel angular (ECA) processing to improve the mechanical properties of magnesium alloys by modifying the microstructure (i.e., reducing the grain size and heterogeneity.) The grain structure of bulk magnesium alloys was successfully modified and the elevated temperature ductility (e.g., superplasticity) improved early in the project. Later, a report published by a Japanese group led us to consider the possibility that the room-temperature ductility could be improved by ECA processing by reducing the crystallographic texture. We were able to duplicate the improvement in ductility; however, we found that the crystallographic texture of the samples was stronger than the initial texture. This sparked a renewed interest in the potential to improve the properties of magnesium alloys through texture modification.

This year the possible texture evolutions of five different wrought alloys—AZ31, AZ80, ZK60, WE43—and an experimental alloy containing 4 wt% Li were cataloged. These alloys were processed at a range of temperatures, different starting microstructures and textures, and a range of processing routes. The result of the study is an extensive database of texture evolutions. For the purpose of this short report, the results are described in Table 3. A couple of examples of the textures are shown in Figure 9. Another finding was that the texture throughout a sample is a strong function of position, particularly after processing by so-called route B (where the samples are rotated 90° between subsequent passes through the ECA die.) Analysis of how the deformation is actually introduced into a representative billet (Figure 10) has begun, and the differences in the textures from different parts of the samples can now be rationalized.

References

1. F. E. Hauser, P. R. Langdon, J. E. Dorn, "Fracture of Magnesium Alloys at Low Temperature," *J Metals, Trans. AIME*, **206**, 589–93 (1956).

Table 3. Summary of texture evolution of 5 magnesium alloys during ECA processing

Alloy	Initial state	T (°C)	Route	Pass	Texture description	Peak (002)	Classification
AZ31	Plate	300	A	1	(002) tilted forward	~6	High temp, Al
				2	“	~8	“
				4	“	~8	“
				8	“	~8	“
“	Extru	200	A	1	(002) tilted backward	~6	Low temp, Al
				2	“	~6	“
				4	“	~6	“
“	As-cast	200	A	1	(002) tilted backward	~6	“
AZ80	Extru	200	A	1	(002) tilted backward	~6	“
ZK60	Extru	260	A	1	(002) vertical, FPN	~4	High temp, Zr
				2	(002) vertical	~6	“
				4	“	~6	“
				8	“	~8	“
WE43	Extru	325	A	2	(002) vertical, FPN	~4	“
				4	“	~4	“
Mg4Li	Extru	260	A	1	(002) vertical		Li alloy
				2	(002) vertical, FPN		“
				4	(002) FPN, vertical		“
ZK60	Extru	260	C	2	(002) tilted forw, back	~4	High temp, Zr
“	“	“	“	4	“	~6	“
ZK60	Extru	260	B	4	(002) tilted forw, back	~4	“
AZ31	Extru	200	B	2	(002) tilt back, vertical	~6	Low temp, Al
“	“	“	“	8	(002) tilted back	>10	“
“	Cast	“	“	2	“	>10	“
AZ80	Extru	200	B	2	(002) tilt back, vertical	~6	“
“	“	“	“	4	“	~6	“
“	“	“	“	8	“	>10	“

2. N. Ono, K. Nakamura, S. Miura, “Influence of Grain Boundaries on Plastic Deformation in Pure Mg and AZ31 Mg alloy Polycrystals,” *Mater. Sci. Forum*, **419–422**, 195–200 (2003).

Publications and Presentations

S. R. Agnew, “Wrought Magnesium: A 21st-Century Outlook,” *JOM* **56**(5), 20–21 (2004).

S. R. Agnew and O. Duygulu, “Plastic Anisotropy and the Role of Non-basal Slip in Magnesium Alloy AZ31,” accepted for publication in *Inter. J. Plasticity* in 2005.

S. R. Agnew, J. A. Horton, T. M. Lillo, and D. W. Brown, “Enhanced Ductility in Strongly Textured Magnesium Produced by Equal Channel Angular (ECA) Processing,” *Scripta Mater.* **50**, 377–381 (2004).

S. R. Agnew, C. N. Tomé, and D. W. Brown, “The Effect of Texture on the Deformation Mechanisms of AZ31B,” presented at Symposium on

Phase Transformations and Deformation in Magnesium Alloys, TMS Annual Meeting, Charlotte, NC, March 16, 2004.

A. L. Bowles, H. Dieringa, C. Blawert, N. Hort, K. U. Kainer, “Investigations in the Magnesium-Tin System,” in *Proceedings of the International Conference on Magnesium—Science, Technology and Applications*, Beijing, China.

A. L. Bowles, H. Dieringa, C. Blawert, N. Hort, K. U. Kainer, “Investigations in the Magnesium-Tin System,” presented at International Conference on Magnesium—Science, Technology and Applications, Beijing, China, September 20–24, 2004.

O. Duygulu and S. R. Agnew, “TEM Investigation of Dislocation Mechanisms in Mg Alloy AZ31B Sheet,” pp. 61–66 in *Magnesium Technology 2004*, Ed. A. A. Luo, TMS, Warrendale, PA, 2004.

O. Duygulu and S. R. Agnew, “TEM Investigation of Dislocation Mechanisms in Mg Alloy

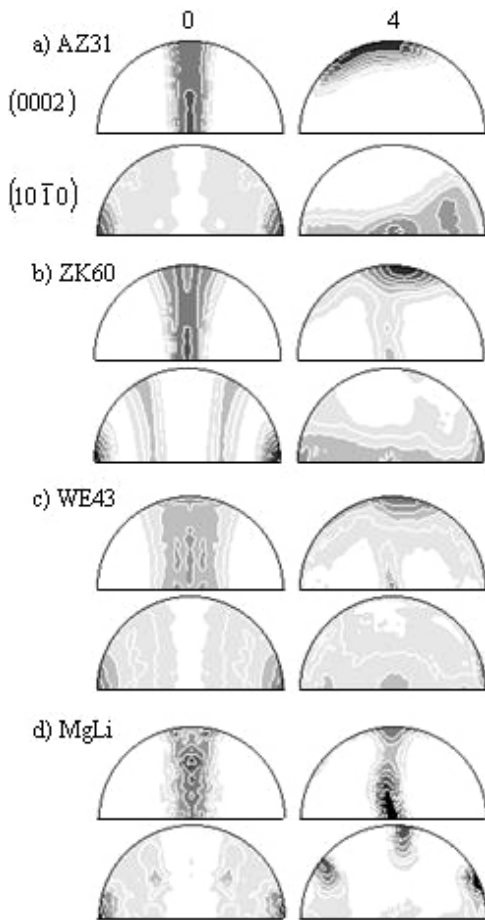


Figure 9. Representative textures from conventional extrusion, labeled 0, and the effect of 4 passes of ECA extrusion, labeled 4. Note strong differences between four of the alloys examined (a) AZ31, (b) ZK60, (c) WE43, and (d) Mg-4 wt % Li despite similarity of initial extrusion textures. Contours are on a logarithmic scale with a maximum (black) of eight multiples of a random distribution.

AZ31B Sheet,” presented at Magnesium Technology 2004 Symposium, 2004 TMS Annual Meeting, Charlotte, NC, March 16, 2004.

J. A. Horton, C. A. Blue, S. R. Agnew, and T. Muth, “Infrared Processing of Wrought Magnesium Alloys,” presented at Magnesium Technology 2004, TMS Annual Meeting, Charlotte, NC, March 16, 2004.

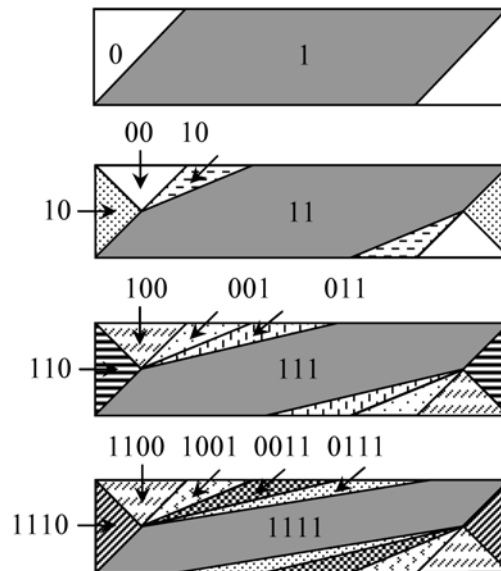


Figure 10. Schematics of the deformed regions of billets after 1, 2, 3, and 4 route A passes through the die, emphasizing the shrinking region, which is completely deformation. (1’s and 0’s indicate strained and unstrained portions during a given pass. For example, 1011 indicates the region was strained during the 1st, 3rd, and 4th passes, but not the 2nd.)

P. K. Liaw, G. M. Stoica, L. J. Chen, E. A. Payzant, C. Xu, T. G. Langdon, and D. E. Fielden, “Plastic Flow and Mechanical Behavior of Some Mg- and Al- Alloys Deformed by Equal Channel Angular Pressing,” presented at Third International Symposium on Ultrafine Grained Materials, TMS Annual Meeting, Charlotte, NC, March 16, 2004.

G. Song, A. L. Bowles, and D. H. StJohn, “Effect of Aging on Yield Stress and Corrosion Resistance of Die Cast Magnesium Alloy,” in *Proceedings of the International Conference on Magnesium—Science, Technology and Applications*, Beijing, China.

G. Song, A. L. Bowles, and D. H. StJohn, “Effect of Aging on Yield Stress and Corrosion Resistance of Die Cast Magnesium alloy,” presented at International Conference on Magnesium—Science, Technology and Applications, Beijing, China, September 20–24, 2004.

C. Equal Channel Angular Extrusion of Soft Ferromagnetic Materials

Principal Investigator: R. B. Schwarz

Los Alamos National Laboratory

MST-8, Mail Stop G755, Los Alamos NM 87545

(505) 667-8454; e-mail: rxzs@lanl.gov

Co-Investigators: T. D. Shen, J. D. Thompson, J. I. Archuleta (LANL), and K. Mukherjee (UC-Davis)

Technology Development Area Specialist: Sidney Diamond

(202) 586-8032; fax: (202) 586-1600; e-mail: sid.diamond@ee.doe.gov

Field Technical Manager: Philip S. Sklad

(865) 574-5069; fax: (865) 576-4963; e-mail: skladps@ornl.gov

Contractor: Los Alamos National Laboratory

Contract No.: W-31-109-Eng-38

Objective

- Conduct research on the theory, synthesis, and properties of soft ferromagnetic alloys having the potential to improve the efficiency of energy conversion devices in the U.S. transportation industry.

Approach

- Use mechanical alloying (MA) (a high-energy ball milling technique) to prepare Fe-rich alloy powders.
- Characterize the powder by X-ray diffraction, scanning differential calorimetry, and magnetometry.
- Consolidate the mechanically alloyed powders by equal-channel angular extrusion and spark-plasma sintering.
- Characterize the compacted alloys by ac and dc magnetic measurements.

Accomplishments

- Prepared nanocrystalline Fe-Al-Si powders by MA. We used differential scanning calorimetry and X-ray diffraction to determine the optimal annealing parameters for reducing the residual stress in the Fe-Al-Si powders, while maintaining the crystallite size below 20 nm, as required for soft ferromagnetic properties.
- Demonstrated that minimizing the magnetic coercivity requires annealing within a narrow temperature window at which residual stresses are eliminated, yet grain growth is avoided.
- Analyzed the effects of crystallite size and residual stress on the magnetic properties.
- Studied the consolidation of our mechanically alloyed Fe-Al-Si powders by spark plasma sintering (collaboration with Professor A. K. Mukherjee at the University of California, Davis).
- Measured the magnetic properties of Fe-Al-Si alloys in both powder and consolidated form.

Introduction

There is continued interest in increasing the efficiency of electrical energy-conversion devices.¹ Here we are interested in ferromagnetic cores of motors and transformers and in magnetic material for

switched-mode power supplies. The challenge for low-loss transformer applications is to develop ferromagnetic materials that have low coercivity, H_C , and high magnetic saturation, M_S . The challenge for efficient switched-mode power supply inductors is

to develop ferromagnetic alloys with high saturation flux density, low permeability, and low losses at high frequencies.

For the first application, the best results have been obtained with two-phase alloys consisting of nanosized *bcc* Fe particles embedded in an amorphous alloy matrix. Two nanocrystalline alloys, known under the trade names Nanoperm² and Finemet,³ are prepared by the partial crystallization of 30- to 50- μm -thick rapidly quenched glassy ribbons. The saturation magnetization of these materials is approximately 1.4 T. Their main drawback is their thinness of gauge and brittleness, which are not optimal for the construction of power transformers.

For the second application, industry has relied extensively on gapped ferrite cores and on “distributed-gap” cores made from pressed ferromagnetic powder or powder cast into a polymer. The last method has the advantage of a low manufacturing cost.

In the present project, we are investigating the synthesis and magnetic properties of *nanocrystalline* ferromagnetic alloys. We prepare these alloys in powder form using mechanical alloying. We then consolidate them using a spark-plasma sintering technique.

Magnetic Properties of Nanocrystalline Ferromagnetic Fe₉₂Al₂Si₆ Alloy Powders

The synthesis of nanocrystalline alloy powders by MA was described in the FY 2003 report and thus will not be repeated here. In that earlier report, we also described the magnetic properties of Fe₈₀Cu₂₀ alloys prepared by MA. We then proposed to continue this work by studying the magnetic properties of Fe-Al-Si alloys. The reason for choosing this alloy was to raise the temperature at which one obtains optimal magnetic properties upon annealing, and to have an alloy of lower magnetostriction.

We used MA to prepare Fe₉₂Al₂Si₆ alloy powders. The as-prepared alloy powders have residual stresses, which have a detrimental effect on the magnetic properties of the alloy. The residual stresses must be eliminated through careful annealing.

In the present study, it is imperative to have accurate measures of the residual stresses and of the crystallite size (more accurately, the size of crystalline domain that diffracts coherently). Most research

to date has deduced these two quantities from an analysis of X-ray diffraction data using the Williamson-Hall method. In this method, for each Bragg reflection, the peak-width-at-half-maximum is plotted as a function of the scattering vector. The crystallite size and residual strain follow from the intercept and slope of a straight line plotted through the data. Figure 1(a) shows that the Williamson-Hall plot is inaccurate because the data have excessive scatter. The problem is that the Williamson-Hall method does not take into account the elastic anisotropy of the crystal, which affects each of the Bragg reflections differently. We used the recent methods of Ungar and co-workers⁴ to calculate the contrast factors, *C*, needed to take into account the anisotropy. Figure 1(b) shows the modified plot. Here, all the diffraction data fit nicely a straight line. We used this method to analyze the diffraction data as a function of annealing temperature.

Figure 2 shows the crystallite size *D*, square root of the dislocation density (proportional to the residual strain ϵ), and coercivity *H_c* as a function of annealing temperature *T_a* for 1-h anneals. Each datum is for a different powder aliquot annealed at the stated temperature. The coercivity was measured using a well-calibrated superconducting quantum-interference device (SQUID), which has an accuracy of approximately ± 0.1 Oe. Annealing causes a monotonic decrease in the residual strain and a monotonic increase in the crystallite size. The coercivity, however, first decreases, reaching a sharp minimum for *T_a* $\approx 450^\circ\text{C}$, and then increases for higher annealing temperatures. Notice the sharp minimum in the coercivity. We detected no phase separation on heating the Fe₉₂Al₂Si₆ alloy up to 600°C . Thus the increase in *H_c* after annealing above 450°C is due to the increase in *D*.

Our data demonstrate that in nanostructured materials, the coercivity *H_c* depends not only on the grain size *D* (as assumed by earlier theories) but also on the residual stress. This is a new result, as we explain next.

Previous research on the magnetic properties of nanocrystalline alloys addressed the dependence of coercivity on grain size. In an extensively quoted paper, Herzer⁵ proposed an explanation for the often observed decrease in the coercivity, $H_c \propto D^6$, for grain sizes below approximately 30 nm. Guided by this theory, researchers have studied nanostructured ferromagnetic alloys without paying attention to the residual stresses in the alloys. Although the residual

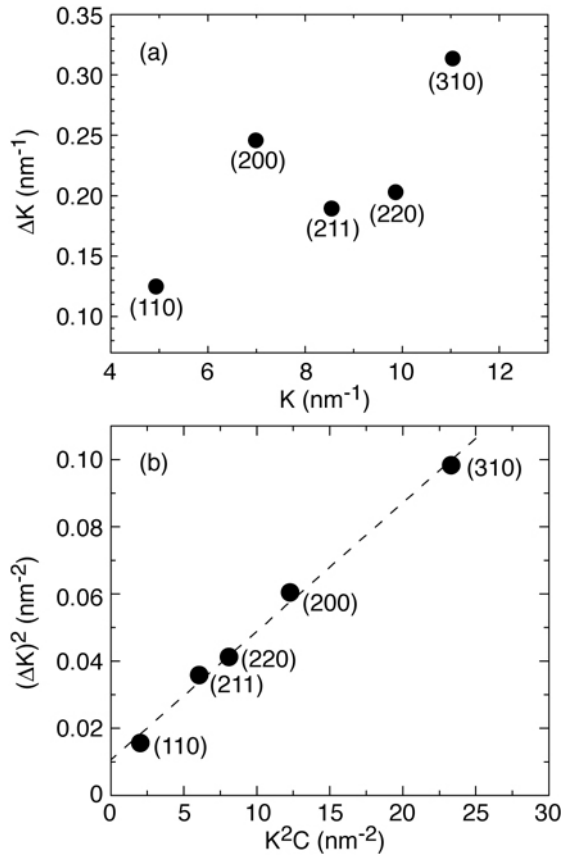


Figure 1. Peak width at half maximum, ΔK , as a function of wavenumber, K , for as-mechanically-alloyed $\text{Fe}_{92}\text{Al}_2\text{Si}_6$ powder: (a) using the Williamson-Hall method, and (b) using contrast-factors, C , according to Ungar [ref. 4].

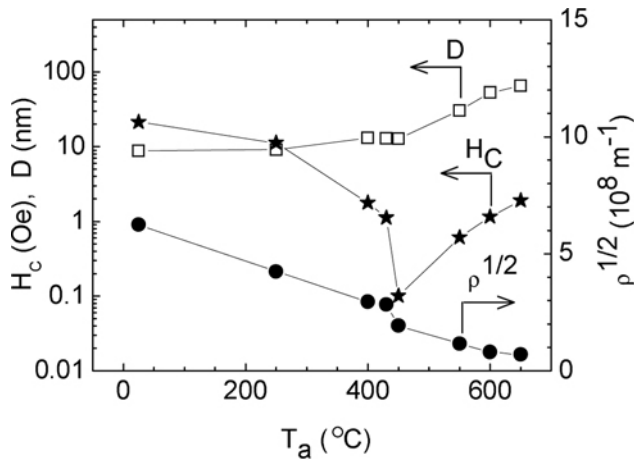


Figure 2. Crystallite size, D , coercivity, H_c , and residual strain, ϵ , (proportional to the square root of the dislocation density, ρ) in mechanically alloyed $\text{Fe}_{92}\text{Al}_2\text{Si}_6$ powder as a function of annealing temperature. The annealing time is 1 h.

stress is low in rapidly quenched ribbons, it cannot be neglected in alloy powders prepared by mechanical alloying.

The data in Figure 2 suggest two magnetic regimes. For $T_a < 450^\circ\text{C}$, the decrease in coercivity is dominated by the residual stress in the material; and for $T_a > 450^\circ\text{C}$, the increase in coercivity is due to the increase in the crystallite size D .

The residual stress in our nanocrystalline alloys is of two types, *microstress* and *macrostress*. The microstresses are generated by dislocation walls that delimit the crystallite size D . The macrostresses are present because the total stress must average to zero. Because the microstress distribution is dominated by compressive components, the macrostress is dilatational in nature, as we confirmed by X-ray diffraction. Annealing facilitates the motion of the dislocations, leading to dislocation polygonization and/or annihilation. This process decreases both the microstresses and macrostresses.

We have measured the residual microstress and macrostress independently. The *microstress* is proportional to the measured square root of the dislocation density and causes a broadening of the Bragg peaks. The *macrostress* is proportional to the overall lattice expansion, which causes a homogeneous shift of *all* the Bragg peaks versus diffracting angle. Figure 3 shows the macrostress in our Fe-Al-Si alloy powder as a function of annealing temperature. Notice that the macrostress vanishes at an annealing temperature of approximately 500°C . The microstress, deduced from the width of the Bragg peaks, shows a very similar dependence on annealing temperature.

An important result to emerge from this work is that the coercivity correlates with the macrostress and not with the microstress. The reason is that the first Fourier component of the microstress distribution (the most important component) is shorter than the magnetic exchange length, L_{ex} . This is to be expected because the crystallite size is less than 20 nm, whereas L_{ex} is about 30 nm. Thus the motion of the magnetic Bloch walls is impervious to the presence of the random short-range microstresses. The domain walls do interact with the long-ranged macrostresses. Therefore, to obtain a magnetically soft nanocrystalline material, one has to first and foremost anneal out the macrostresses. However, the annealing temperature cannot be increased too much. Indeed, the data in Figure 2 show that annealing above 450°C causes an increase in the crystallite

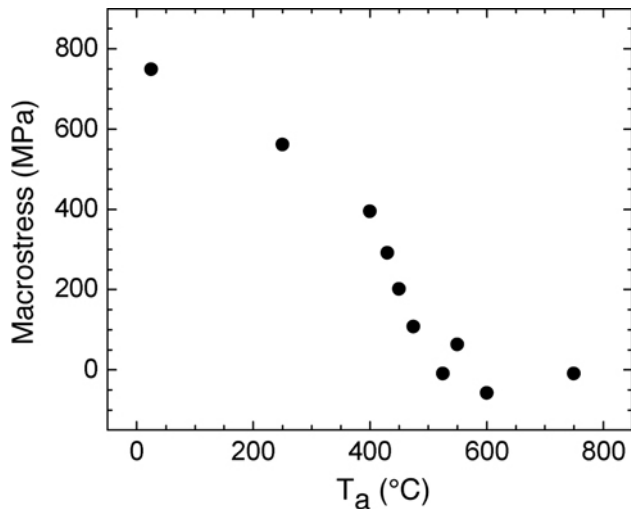


Figure 3. Macrostress in mechanically alloyed $\text{Fe}_{92}\text{Al}_2\text{Si}_6$ powder as a function of annealing temperature. The annealing time for each sample was 1 h.

size D . When D becomes comparable in size to L_{ex} , then the coercivity increases rapidly because now the range of the microstresses becomes comparable to L_{ex} . Then the coercivity increases proportionally to D^6 , as predicted by the random anisotropy model.^{5,6}

Magnetic Properties of Consolidated Nanocrystalline Ferromagnetic $\text{Fe}_{92}\text{Al}_2\text{Si}_6$ Alloy Powder

The mechanically alloyed $\text{Fe}_{92}\text{Al}_2\text{Si}_6$ powder was consolidated by spark-plasma-sintering at UC-Davis. In this technique, the powder is first cold pressed to about 300 MPa and heated to approximately 700°C. A series of current pulses are then sent through the compressed powder. The current heats preferentially the contact points between the particles, accelerating the sintering process. The consolidated disks were approximately 90% dense.

The consolidated disks were cut (at Los Alamos National Laboratory) to prepare small toroid-shaped specimens. Primary and secondary solenoids were added to the toroids to create small transformers on which to measure magnetic properties.

Figure 4 shows the B-H curve for such a toroid. The saturation magnetization is approximately 1.6 T, and the coercivity is approximately 4 Oe. The coercivity, although low compared with that of any ferromagnetic powder prepared by MA, is still too high for it to be used in ferromagnetic cores of low-loss transformers and motors. We attribute the finite co-

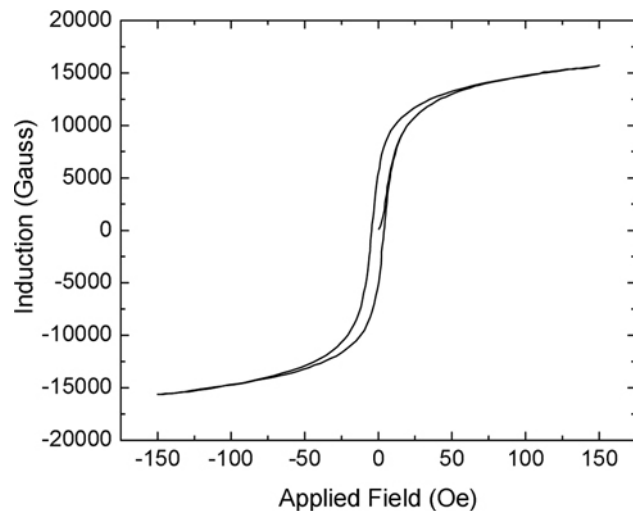


Figure 4. Induction, B , as a function of applied field, H , in a toroid-shaped sample made from $\text{Fe}_{92}\text{Al}_2\text{Si}_6$ powder. The toroid was cut from a bulk disk made by consolidating the powder using spark-plasma-sintering at UC-Davis.

ercivity to the presence of macrostresses introduced during the consolidation process. These macrostresses have not been reduced by annealing. In addition, during the consolidation at 700°C, the grain size grows to above 100 nm.

Future Research

1. Optimize the temperature used during the spark-plasma-sintering consolidation to minimize the grain growth.
2. Study the influence of post-annealing on reducing the macrostresses introduced during consolidation.
3. Optimize the composition of the Fe-Al-Si to minimize the magnetostriction and magneto-crystalline anisotropy.
4. Study the magnetic properties of two-phase materials consisting of $\text{Fe}_{92}\text{Al}_2\text{Si}_6$ powder with nanosize grains and a ferromagnetic “glue” consisting of an amorphous ferromagnetic alloy with a glass transition temperature lower than 450°C. The $\text{Fe}_{92}\text{Al}_2\text{Si}_6$ alloy should provide a high saturation magnetization, whereas the amorphous phase will deform during sintering, closing the gaps and producing a fully dense ferromagnetic alloy.

Acknowledgment

This work was supported by the DOE Office of FreedomCAR and Vehicle Technologies.

References

1. U.S. Department of Energy, "Annual Energy Review 2001," from www.eia.doe.gov.
2. A. Kojima, H. Horikiri, Y. Kamamura, A. Makino, A. Inoue, and T. Matsumoto, "Production of Nanocrystalline bcc Fe-Nb-B Bulk Alloys by Warm Extrusion and Their Magnetic Properties," *Mater. Sci. Eng. A* **179/180**, 511 (1994).
3. Y. Yoshizawa, S. Oguma, and K. Yamauchi, "New Fe-based Soft Magnetic Alloys Composed of Ultrafine Grain Structure," *J. Appl. Phys.* **64**, 6044 (1988).
4. T. Ungar, I. Dragomir, A. Revesz, and A. Borbely, "The Contrast Factors of Dislocations in Cubic Crystals: The Dislocation Model of Strain Anisotropy in Practice," *J. Appl. Cryst.* **32**, 992 (1999).
5. G. Herzer, in *Handbook of Magnetic Materials*, vol. 10, ed. K. H. J. Buschow, Elsevier Science B. V., Amsterdam, 1997, chap. 3.
6. G. Herzer, "Grain Size Dependence of Coercivity and Permeability in Nanocrystalline Ferromagnets," *IEEE Trans. Magn.* **26**, 1397 (1990).

Publications and Presentations

T. Li, F. Grignon, D. J. Benson, K. S. Vecchio, E. A. Olevsky, F. Jiang, A. Rohatgi, R. B. Schwarz, and M. A. Meyers, "Modeling the Elastic Properties and Damage Evolution in Ti-Al₃Ti Metal-Intermetallic Laminate (MIL) Composites," *Mater. Sci. and Eng. A* **374**, 10–26 (2004).

R. B. Schwarz, "Synthesis and Properties of Ferromagnetic Bulk Metallic Glasses," MST Division Seminar, Argonne National Laboratory, November 7, 2003.

R. B. Schwarz and T. Lillo, "Metal-Intermetallic Composites Prepared by Melt Reaction Synthesis," presented at the Workshop on Ceramics Ductilization, Los Alamos National Laboratory, November 15–18, 2004.

R. B. Schwarz and T. D. Shen, "High-Strength, High Conductivity Bulk Nanostructured Alloys," invited presentation at the Symposium on Processing and Properties of Structural Nanomaterials, 2003 TMS Fall Meeting, Chicago, November 9–12, 2003.

R. B. Schwarz, T. D. Shen, U. Harms, and T. Lillo, "Soft Ferromagnetism in Amorphous and Nanocrystalline Alloys," *Journal of Magnetism and Magnetic Materials* **283**, 223–230 (2004).

R. B. Schwarz, T. D. Shen, T. Lillo, G. D. Zhan, and A. K. Mukherjee, "Soft Ferromagnetism in Nanocrystalline Alloys," invited presentation at the 10th International Symposium on Metastable, Mechanically Alloyed and Nanocrystalline Materials (ISMAM 2003), Foz do Iguacu, Brazil, August 22–26, 2003.

T. D. Shen, U. Harms, and R. B. Schwarz, "Bulk Fe-based Metallic Glass with Extremely Soft Ferromagnetic Properties," *Materials Science Forum* **386–388**, pp. 441–446 (2002).

Awards

R. B. Schwarz was awarded the Von Humboldt Research Award for Senior U.S. Scientists for his research and teaching and was awarded the ISMANAM Medal for research in amorphous and nanocrystalline crystals at the International Symposium on Metastable, Mechanically Alloyed, and Nanocrystalline Materials.

D. Equal Channel Angular Extrusion Processing of Alloys for Improved Mechanical Properties

Principal Investigator: Thomas M. Lillo
Idaho National Engineering and Environmental Laboratory
MS2218, P.O. Box 1625, Idaho Falls, ID 83415-2218
(208) 526-9746; fax: (208) 526-4822; e-mail: tml@inel.gov

Technology Development Area Specialist: Sidney Diamond
(202) 586-8032; fax: (202) 586-1600; e-mail: sid.diamond@ee.doe.gov
Field Technical Manager: Philip S. Sklad
(865) 574-5069; fax: (865) 576-4963; e-mail: skladps@ornl.gov

Contractor: Idaho National Engineering and Environmental Laboratory
Contract No.: DE-AC07-99ID13727

Objective

- Investigate equal channel angular extrusion (ECAE) as a deformation processing technique to improve material properties such as strength, formability, fatigue, and corrosion.
 - Apply ECAE processing to produce advanced, lightweight materials with enhanced formability, higher strength-to-weight ratio, and higher stiffness, ultimately leading to reductions in vehicle weight and thus more fuel-efficient vehicles.

Approach

- Assess the effects of ECAE processing parameters on the mechanical properties of a magnesium alloy (ZK60A) and an aluminum metal matrix composite (MMC) (AL6061+B₄C). Both are lightweight alloys with potential for use in lightweight structural applications in vehicles.
- Determine the optimum ECAE processing schedule for the maximum increase in mechanical properties.
- Characterize the microstructure and mechanical properties of the ECAE-processed material.
- Use microstructure and mechanical properties data to model the flow stress of materials processed with ECAE.

Accomplishments

- ECAE-processed five billets of ZK60A using new ECAE processing schedules and temperatures.
 - CAE-processed eight billets of AL6061 + 10 wt% B₄C using new ECAE processing schedules and temperatures.
- Characterized microstructure and mechanical properties of ECAE-processed AL6061+10 wt% B₄C.
 - Improved ductility (>10% in some cases) and increased the modulus of elasticity from 70 GPa to over 85 GPa, and in some cases >100 GPa, of AL6061+10 wt% B₄C.
- Performed strain rate jump tests on ECAE-processed ZK60A to determine superplastic behavior.
 - Characterized the microstructure of various ECAE-processed and annealed brasses using orientation imaging microscopy (OIM) in support of flow-stress modeling work.

Future Direction

- Complete the superplastic behavior study of ECAE-processed ZK60A.
 - Understand the variation in elastic modulus and tensile strength of MMCs with ECAE processing parameters through further ECAE processing, microstructural characterization, and mechanical testing.
 - ECAE process an AL6061+ 20wt% B₄C MMC, as well as other MMCs, and evaluate mechanical properties to demonstrate the universal improvement in the mechanical properties associated with ECAE processing.
 - Determine the modifications in ECAE die design and ECAE furnace design to ECAE process titanium-based MMCs.
 - Continue ECAE processing, characterization of microstructure, and characterization of mechanical properties in support of flow-stress modeling.

Introduction

Over the past years, this ECAE program has studied ECAE processing (Figure 1) of a wide variety of materials, from pure metals to alloys and MMCs. Initially it was surmised that ECAE processing might be a method of producing bulk nano-crystalline materials through grain refinement

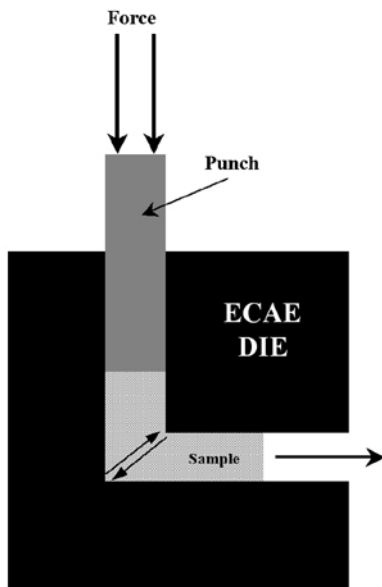


Figure 1. Schematic of ECAE processing.

associated with intense plastic deformation. Microstructural development and mechanical properties were tracked as a function of ECAE processing parameters such as processing route (Figure 2), number of passes through the ECAE die, processing temperature, and the level of back

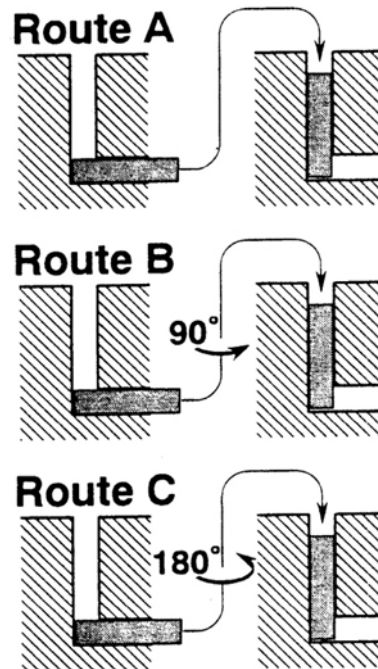


Figure 2. Schematic illustrating sample rotation between subsequent passes through the ECAE die.

stress during processing. A nano-crystalline grain size was difficult to obtain in most materials. Typically, the grain size stabilized after relatively few (4–10) passes through the ECAE die at a value determined by the metal or alloy being processed and the ECAE processing temperature. Although this grain size was generally sub-micron, it was not nano-crystalline (≤ 100 nm). Furthermore, the grain boundary structures were not in stable equilibrium; and the property improvements exhibited by ultra-fine-grain materials made by other methods were not realized in ECAE-processed materials.

However, most materials exhibited significant improvements in their mechanical properties as a result of ECAE processing with a subsequent annealing procedure. One example with potential lightweight vehicle applications was a commercial magnesium alloy ZK60A (Mg-5% Zn-0.5% Zr). During FY 2003, it was found that, with the appropriate combination of ECAE parameters, ZK60A could be ECAE-processed to a final grain size of 1–2 μm . Alloys in this grain size range have been known to exhibit superplastic behavior. A subsequent superplastic study of this ECAE-processed material showed elongations of >200% at 200°C and a strain rate of $10^{-3}/\text{sec}$. Since this was a first attempt, part of the focus during FY 2004 was to optimize the ECAE-processing schedule to obtain superplasticity at higher strain rates.

Another material found to benefit from ECAE processing was an experimental MMC, AL6061 with 10 wt% B_4C particles, obtained from Dynamet Technologies. Dynamet desires to develop lightweight materials with high stiffness for structural applications. The composite was made by powder metallurgy techniques and suffered from very low ductility (virtually zero) and little enhancement to the stiffness over commercial AL6061. However, elongations as high as 10% and improvements to the stiffness (>10%) were found after ECAE processing. The elastic modulus (~80 GPa) was still significantly below the theoretical value of ~110 GPa.

Again, since this was a first attempt, a portion of FY 2004 was devoted to exploring the optimization of ECAE processing to obtain greater improvements in the mechanical properties of this composite. Furthermore, work on this alloy will be useful in the processing of titanium MMCs that have greater application for lightweight, high-strength structural applications. Titanium MMCs will require modifications to the ECAE die and furnace, so the AL6061 composite is used to demonstrate proof-of-principle.

Work in support of the effort to model the flow stress of metals and alloys also continued during FY 2004. ECAE processing produces very fine-grain-size materials—finer than previously obtained by rolling, for instance. Determination of the relationship between flow stress and grain size at very small grain sizes aids in the elucidation of flow stress behavior. The data will eventually be integrated into a model capable of predicting grain size development and the resulting mechanical

properties of thermomechanically-processed materials.

Previous flow stress modeling work raised issues of the effect of stacking fault energy on the flow stress behavior. To answer these questions, various brasses, ranging from 30 to 5% Zn, with widely varying stacking fault energies, were ECAE-processed and annealed to obtain a wide range of grain sizes. The microstructure was analyzed during FY 2004, and the flow stress behavior of these materials was determined and related back to the developing flow stress model.

ECAE Processing of Magnesium Alloys

Previously, commercial-grade ZK60A (Mg-5% Zn-0.5% Zr) was ECAE-processed using three different sets of parameters:

- Four passes by the B-route at 260°C and no applied back stress
- Four passes by the B-route at 150°C and 18.3 ksi back stress
- Six passes by the B-route at 150°C and 18.3 ksi back stress

The results of the superplastic study on these samples seemed to indicate that lower ECAE temperatures and more passes through the die correlated with improvements in superplastic behavior. Therefore, new ECAE processing schedules, incorporating these insights, were devised. Specifically, billets were processed according to Table 1.

Table 1. ZK60A ECAE processing schedules

Sample	Initial billet condition	ECAE temperature (°C)	ECAE route	Back stress level, ksi
1	T5	150	8B	15.1
2	T5	150	2B	15.1
		135	1B	15.1
		120	1B	19.7
3	T5	150	2B	15.1
		130	4B	15.1
4	Solution treated	200	2B	10.6
		150	6B	21.2
5	T5	150	2A	15.1

Sample 1 explored the effect of the number of passes through the ECAE die on superplastic behavior; Sample 2 looked at ECAE processing temperature; and Sample 3 was processed with a combination of both variables. Sample 4 attempted

to look at the effect of precipitation from solid solution during ECAE processing, and Sample 5 was to evaluate the uniformity of strain in the billet. At this time, tensile bars have been made and strain rate jump tests performed at 180, 225, 250 and 275°C on Samples 1–4. The strain rate sensitivity factor, m , was calculated from:

$$m = \log(\sigma_2/\sigma_1)/\log(\dot{\epsilon}_2/\dot{\epsilon}_1), \quad (1)$$

where $\dot{\epsilon}$ was the strain rate, σ was the flow stress and the subscripts 1 and 2 referred to the values before and after the strain rate jump, respectively. The m factors are plotted in Figure 3 as a function of strain rate for the test temperatures. (The strain rates in the plots are taken as the average of the strain rate before and after the strain rate jump.) Superplastic behavior is associated with m values near 0.5. At 250 and 275°C, all samples behaved similarly, and presumably rapid grain growth out of the superplastic regime was occurring. At the two lower temperatures (180 and 225°C), only sample 4 showed significantly different behavior across the strain rates investigated. Sample 4 exhibited $m \approx 0.5$ around a strain rate of $\sim 10^{-2} \text{ sec}^{-1}$ at 225°C. The other samples exhibited $m \approx 0.5$ only at very low strain rates at all temperatures studied. Sample 4 was ECAE-processed in the solutionized state, and precipitation occurred during processing and possibly during testing to produce the different superplastic behavior. Microstructural examination of Sample 4 will be performed to try to assess the effect of ECAE processing on precipitation. Finally, samples will be tested using the most promising combination of temperature and strain rate to determine the maximum elongation possible.

It was also demonstrated during FY 2003 that a modified version of ZK60A (with additions of cerium and yttrium), provided by Daniel Schechtmen at NIST, demonstrated even better superplastic behavior than commercial ZK60A.

Once the optimum ECAE processing schedule is developed and superplastic parameters (temperature and strain rate) are determined for commercial ZK60A, they will be applied to the modified ZK60A and the resulting superplastic behavior documented.

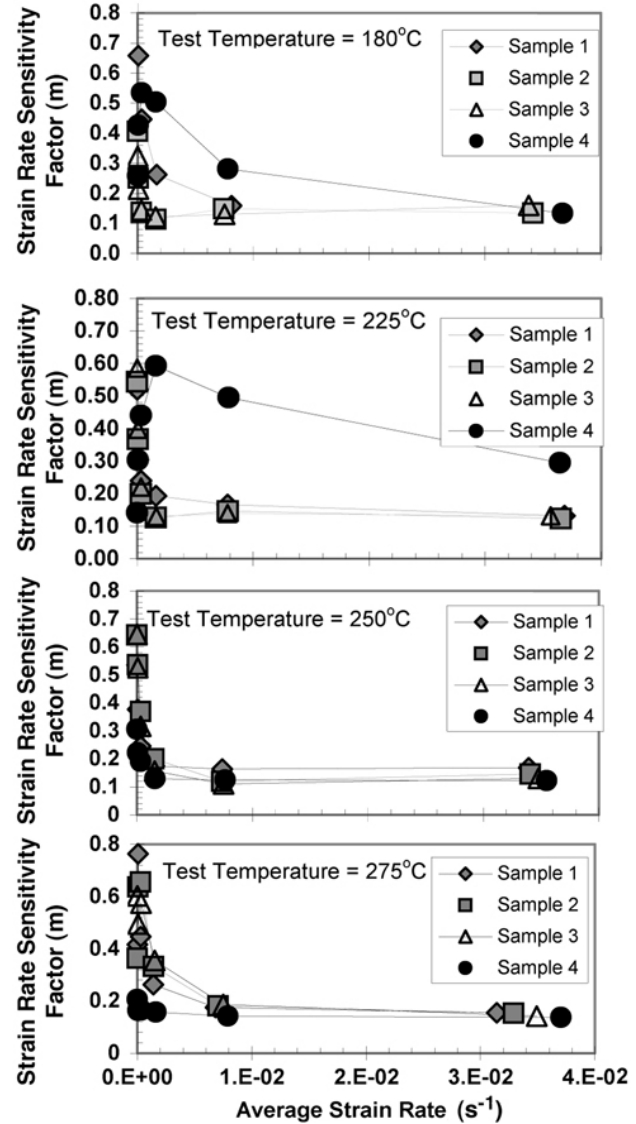


Figure 3. Strain rate sensitivity of ECAE-processed ZK60A at 180 and 225°C.

These preliminary results suggest that it might be possible to develop a high-strain-rate superplastic magnesium alloy. This would facilitate the use of magnesium alloys in automotive applications. Superplastic forming would minimize fabrication waste for this relatively expensive alloy, making it more economically competitive with traditional iron-based materials. High-strain-rate superplastic forming also offers the potential for rapid fabrication, resulting in higher productivity and making this alloy more competitive with conventional materials of construction. Ultimately, vehicles incorporating magnesium alloys would be lighter

than those that rely on traditional alloys, and therefore more fuel-efficient.

ECAE Processing of Aluminum Alloy Composites

Additional billets of prototype MMCs were purchased from Dynamet Technology. The material consisted of an AL6061 matrix with boron carbide particles (~50 μm in diameter on average) present at a level of either 10 or 20 wt %. Additions of B_4C particles increase the stiffness of the AL6061 matrix, making it more suitable for use in lightweight structural applications by reducing the deflection under load. The material was fabricated by powder metallurgy methods and contained agglomerates of boron carbide particles. During FY 2003, it was found that the B_4C particles appeared to be concentrated around prior aluminum alloy powder particles. The interface between adjacent B_4C particles was very weak and acted as a defect during tensile loading, causing premature fracture. The elongation/ductility of these composites was negligible in the as-received state.

During FY 2003, it was found that considerable increases in density, elongation, and elastic modulus could be realized through ECAE processing. Relatively high ECAE processing temperatures closed residual porosity, while lower ECAE processing temperatures eliminated poorly bonded particle/particle interfaces (i.e., dispersed the particles in the agglomerates). Therefore, during the first half of FY 2004, ECAE processing schedules were devised that incorporated initial passes at relatively high temperatures (~300°C) to close porosity, followed by subsequent passes at lower temperatures ($\leq 150^\circ\text{C}$) to disperse B_4C agglomerates.

The specific schedules used are shown in Table 2. The ECAE-processed billets remained intact and were free of cracks and other flaws commonly found in ECAE-processed materials of low ductility. Tensile bars were prepared from each billet and oriented parallel to the ECAE direction.

The density of each tensile bar was determined by the Archimedes principle, and the average density is shown in Table 3. ECAE processing significantly increased the density (~3.5%), but full density still was not achieved. There also is very little difference in density between the different ECAE processing routes.

Table 2. Processing schedules for AL6061+10wt% B_4C

Sample	Initial condition	ECAE temperature ($^\circ\text{C}$)	ECAE route	Back stress (ksi)
B3528-1	T0	300	2A	10.6
		150	4B	22.7
B3528-8	T0	300	2A	10.6
		150	4A	22.7
B3528-10	T0	300	2B	10.6
		150	4B	22.7

Table 3. Effect of ECAE processing on density

Sample	Average density (grams/cm ³)	Relative density ^a (%)
As-received	2.55	94.9
B3528-1	2.64	98.1
B3528-8	2.64	98.1
B3528-10	2.65	98.5

^aThe theoretical density was taken as 2.69 g/cm³, based on a rule-of-mixtures calculation

The tensile bars were heat treated to either the T4 (solid solution) or T6 (optimum aging treatment) condition. (The samples were heat treated to remove the grain size refinement due to ECAE processing. Only the effect of ECAE processing on the B_4C particulate was of interest at this time.) Two tensile tests for each heat treatment condition were run at room temperature for each billet. The results are shown in Table 4. Significant increases in all properties resulted from ECAE processing compared with the as-received material, B3528 AR. Generally, the ductility in the T4 condition is greater than in the T6 condition (~9% vs. ~3%, respectively); but both are much greater than in the as-received material, which exhibited virtually no ductility. The yield and ultimate tensile strength (UTS) increased by more than 30% and 50%, respectively, with the UTS in some cases almost doubling that of the as-received material. The ECAE-processed materials also showed an increase in the yield and ultimate strengths, ~15% and ~5%, respectively, over commercial AL6061 (without B_4C reinforcement). The elastic modulus also increased and, in one case, Sample B3528 1-2, approached the theoretical value (~110 GPa) as calculated by the rule-of-mixtures. Overall, billet B3528-10 exhibited slightly better mechanical properties than billets ECAE-processed by other schedules, although the differences were not great.

Table 4. Mechanical properties of ECAE-processed AL6061+10wt% B₄C

Heat treatment	Specimen ID	Modulus (GPa)	Yield strength (MPa)	UTS (MPa)	Elongation (%)	RA (%)
T4	B3528 1-2	115	158	248	9	10
	B3528 1-6	73	161	208	3	5
	B3528 8-2	59	140	198	3	4
	B3528 8-6	69	161	249	8	10
	B3528 10-2	94	163	260	9	11
	B3528 10-6	97	170	268	7	5
	B3528 AR	56	117	129	0.8	0
	B3528 1-1	75	326	337	2	4
T6	B3528 1-5	88	N/A	314	0.2	2
	B3528 8-1	59	279	298	1.6	1
	B3528 8-5	80	325	331	1.3	2
	B3528 10-1	73	333	351	3	6
	B3528 10-5	83	340	356	3.7	7
	B3528 AR	71	N/A	193	0	0

Although increases in the mechanical properties are observed *on average*, significant variability was observed in specimens from the same billet with the same heat treatment. This condition, most likely, arose from remaining B₄C particle/particle weak interfaces and residual porosity.

The ECAE-processed microstructures were significantly different from the as-received material. Figure 4 compares the microstructures of the as-received and sample B3528-1. The micrographs were taken from samples in the T4 condition and were perpendicular to the extrusion axis. The as-received material had more B₄C agglomerates and voids within the agglomerates (at the arrows in Figure 4a) compared with ECAE-processed material (Figure 4b). Smaller agglomerates and a reduced number of voids were found in the ECAE-processed material. The B₄C particles also were more evenly distributed throughout the material compared with the as-received sample. These factors undoubtedly contributed to the observed increase in mechanical properties. The microstructures of the other ECAE-processed samples showed similar results and indicated the ECAE processing route had little influence on the microstructure. Only the number of passes seemed to significantly affect the boron carbide particle distribution.

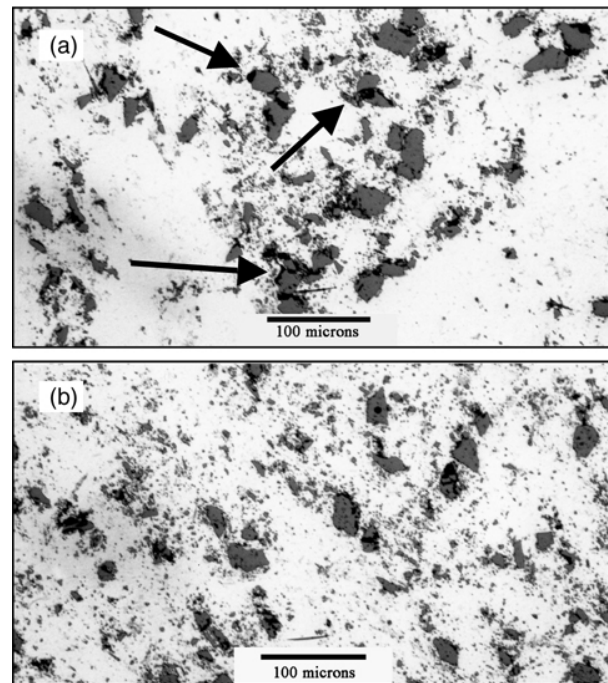


Figure 4. Microstructure of AL6061+ 10 wt% B₄C of the (a) as-received and (b) B3528-1 in the T-4 condition.

Overall, the tensile results in FY 2004 confirmed the preliminary findings obtained in FY 2003 that ECAE can be used to significantly increase the mechanical properties of these MMCs. However, resid-

ual porosity and weak particle/ particle interfaces still existed even after ECAE processing with the new processing schedules. These defects, although greatly reduced, are still thought to adversely affect the mechanical properties. Therefore, new schedules were developed to further reduce residual porosity and eliminate B₄C agglomerates and weak B₄C particle/particle interfaces. Specifically, additional passes were added to the end of those outlined in Table 2 to further redistribute the particles and close any porosity generated during the low-temperature passes through the ECAE die. The elastic modulus was evaluated after various passes using ultrasonic methods. After the fourth pass, very little change in the elastic modulus was observed even up to a total of 8 passes. The elastic modulus stabilized at ~ 80–85 GPa, which is still significantly lower than theoretical for this composite (~110 GPa). Tensile samples will be tested early in FY 2005. The mechanical properties of material processed by simplified ECAE processing schedules (only 4 passes through the ECAE die) also will be determined in early FY 2005 for comparison with previous results. Heat treatment of the ECAE-processed material to promote better bonding of the B₄C particles to the AL6061 matrix will be explored. The goal is to increase the elastic modulus to near theoretical values. Preliminary exploration of titanium MMCs will begin after these experiments and mechanical testing.

ECAE processing of MMCs still appears to have the greatest potential for improving mechanical properties. The improved fabricability of ECAE-processed MMCs may enable the use of these light-weight, high-stiffness materials in more transportation applications for increased fuel efficiency.

Modeling Flow Stress

Brasses with 5%, 10%, or 30% zinc were ECAE processed during FY 2003 and then analyzed during the first half of FY 2004 for microstructure and mechanical properties. The goal is to relate the difference in stacking fault energy with the flow stress behavior. Tensile samples were annealed for 1 hour at 300, 400, and 600°C. Obvious differences in the room-temperature flow stress behavior between the different brasses were found (Figure 5).

Samples were prepared from the failed tensile bars and sent out for OIM and analysis. Among other things, OIM analysis revealed that samples

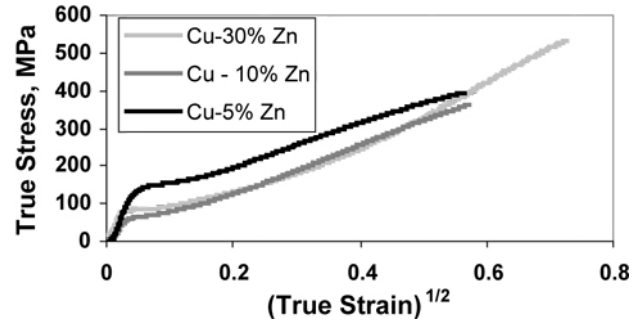


Figure 5. Flow stress behavior of various brasses ECAE-processed and annealed at 600°C for 1 hour.

BR16–1 and –2 were not fully recrystallized; the result was low Σ3 (twin) grain boundary fraction for these samples (Table 5). OIM analysis also revealed that the grain size at a given annealing temperature is influenced by the zinc content—the grain size increases with increasing zinc content. All fully recrystallized samples have a high twin grain boundary fraction (>50%). The OIM data will be combined with the tensile data and analyzed for the flow stress model under development.

The OIM data also revealed one other noteworthy result. The Σ3 grain boundary content for Br2C-14 (700°C, 1 hour) was significantly lower than expected (Table 5). A closer look at the OIM data revealed a fairly high fraction (~28%) of low-angle grain boundaries. Mapping of the low-angle grain boundaries revealed they were mainly associated

Table 5. OIM analysis results for ECAE-processed and annealed brasses

Sample	Description	Grain-size	Σ3 fraction	Total CSL fraction
BR16	Cu-5Zn			
-1	300°C	0.46	0.210	0.240
-2	400°C	0.70	0.361	0.410
-3	600°C	1.44	0.699	0.752
BR17	Cu-10Zn			
-1	300°C	0.57	0.561	0.634
-2	400°C	0.89	0.574	0.621
-3	600°C	11.77	0.593	0.605
BR2C	Cu-30Zn			
-7	400°C	1.73	0.488	0.526
-12	500°C	7.63	0.514	0.529
-8	600°C	20.83	0.592	0.611
-14	700°C	53.24	0.398	0.406

with twin grain boundaries (Figure 6). Three low-angle boundaries associated with twins are shown at the arrows, as examples. The low-angle grain boundaries ($<10^\circ$) are shown in white. The grain boundaries near these low-angle grain boundaries no longer have a twin orientation. Therefore, it would appear that annealing at 700°C leads to the breakup of twin boundaries in this material. This also is shown by Figure 7, where the tolerance for what is considered a twin grain boundary has been varied. Twin boundaries in black represent deviations of up to about 8.7° , while those in white are within 2.9° of the exact twin orientation. For Br2C-8 (600°C , 1 hour), nearly all of the twin boundaries are within 2.9° of the exact twin orientation (Figure 7b), while the twin grain boundaries in the sample annealed at 700°C show relatively large deviations from the exact twin orientation (Figure 7a).

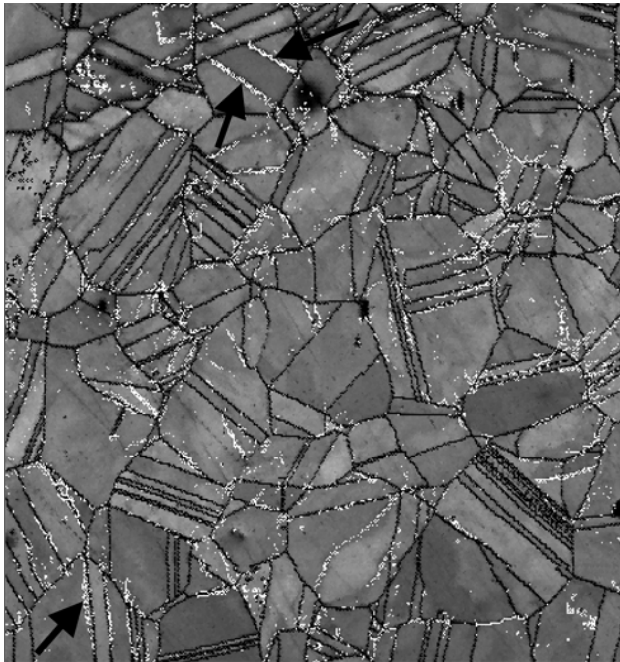


Figure 6. OIM image showing the low-angle grain boundary structure (white lines) in Cu-30% Zn sample annealed at 700°C for 1 hour.

This may provide evidence of twin grain boundaries acting as preferential dislocation sources. Decomposition of twin boundaries at high temperatures leaves behind a low-angle grain boundary and a grain boundary with a misorientation different from the original twin orientation.

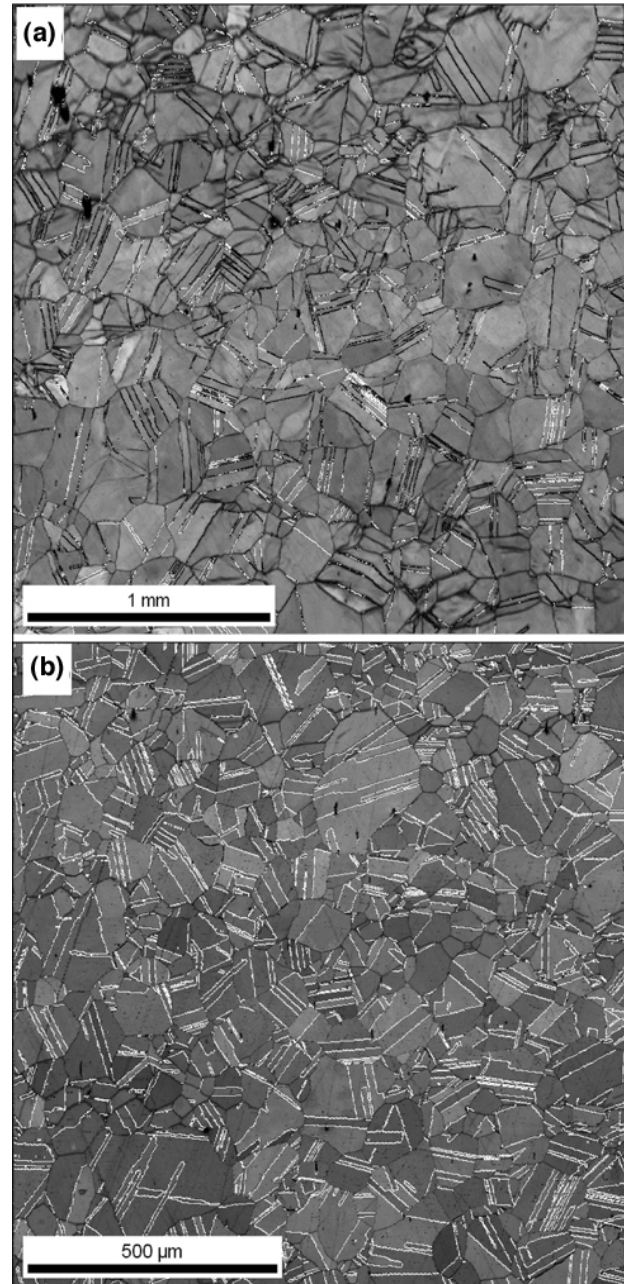


Figure 7. The Cu-30% Zn sample annealed at 700°C (a) exhibits twin boundaries that deviate up to about 9° from the exact twin boundary orientation (black boundaries). Annealing at 600°C (b) results in twin boundaries that deviate by $\leq 3^\circ$ from exact coincidence (white boundaries).

This would support past findings that the flow stress correlates with the twin grain boundary density, implying that twin boundaries act as dislocation sources during deformation. Further analysis of this sample to confirm this finding is under way. The

findings will be published in a peer-reviewed journal.

Conclusions

During FY 2004, work focused on developing ECAE processing schedules to optimize mechanical properties. Billets of a commercial magnesium alloy, ZK60A, have been ECAE processed by five new processing schedules. Preliminary superplastic studies show that the processing schedules may potentially yield a lightweight material capable of high strain rate superplasticity. Such a material will be more economically competitive (high production rate coupled with minimal scrap) with other traditional structural materials such as steel. Considerable weight savings and increased fuel efficiency could be realized by using magnesium alloys in place of iron-based materials.

ECAE processing also appears to be a means of improving the mechanical properties of MMCs. The proper combinations of ECAE processing temperatures, back stress, and the number of passes through the ECAE die result in MMCs with better strength, ductility, and elastic modulus. The elastic modulus is still significantly lower than the theoretical value, and microstructural studies indicate residual porosity, both suggesting that further improvements can be made with optimized ECAE processing schedules. Increased ductility afforded by ECAE process

ing offers the potential for improved fabricability and wider application of MMCs. Lightweight, high-stiffness MMCs may then be employed as structural members in transportation applications, leading to more fuel-efficient vehicles.

Publications and Presentations

S. R. Agnew, J. A. Horton, T. M. Lillo, D. W. Brown, "Enhanced Ductility in Strongly Textured Magnesium Produced by Equal Channel Angular Extrusion," *Scripta Mat.*, **50**, 377–381 (2004).

D. P. Field, M. M. Nowell, P. Trivedi, S. I. Wright, and T. M. Lillo, "Local Orientation Gradient and Recrystallization of Deformed Copper," accepted for publication in *Proceedings of the International Conference on Textures and Anisotropy of Polycrystalline Materials*.

D. P. Field, B. W. True, T. M. Lillo, J. E. Flinn, "Observation of Twin Boundary Migration in Copper During Deformation," accepted for publication in *Materials Science and Engineering A*, 2004.

M. M. Nowell, D. P. Field, S. I. Wright, and T. M. Lillo, "In-Situ EBSD Investigation of Recrystallization in ECAE Processed Copper," *Metals. Sci. Forum*, **467–470**, 1401–1406 (2004).

R. B. Schwarz, T. D. Shen, U. Harms, and T. Lillo, "Soft Ferromagnetism in Amorphous and Nanocrystalline Alloys," *Journal of Magnetism and Magnetic Materials*, **283**, 223–230 (2004).

E. Development of an Advanced Squeeze Casting Process for the Production of High-Integrity Truck Components

Principal Investigator: David C. Weiss

Eck Industries, Incorporated

1602 North 8th Street, Manitowoc, WI 54221-0967

(920) 682-4618; fax: (920) 682-9298; e-mail: dweiss@eckindustries.com

Technology Development Area Specialist: Sidney Diamond

(202) 586-8032; fax: (202) 586-1600; e-mail: sid.diamond@ee.doe.gov

Field Technical Manager: Philip S. Sklad

(865) 574-5069; fax: (865) 576-4963; e-mail: skladps@ornl.gov

Contractor: Eck Industries, Incorporated

Contract No.: 4000022893

Objective

- Develop the equipment and process technology for an advanced squeeze casting (ASC) process to enable production of high-integrity cast metal components.
 - Integrate the advantages of two casting methods—low-pressure permanent mold and direct squeeze casting—to attain non-turbulent fill of the die, high solidification rates to refine microstructural features, and solidification under pressure to minimize microporosity.
 - Design and build a new kind of casting machine and develop process technologies needed to cast high-integrity truck components from nonferrous alloys.

Approach

- Design and construct a casting machine that integrates a low-pressure metal delivery system suitable for either aluminum or magnesium alloys, reliable gate shut-off technology, and direct application of squeeze pressures of up to 103 MPa (15,000 psi). This machine is intended for production.
- Develop a gate shutoff mechanism that will operate reliably in a production environment.
- Select a casting that will be produced in the casting machine built for this project.
- Use fluid-flow and solidification analysis to predict optimum flow conditions for metal entering the mold and differential squeeze pressure requirements.
- Design and build cast tooling.
- Develop process technologies for the low-pressure/squeeze casting of aluminum alloys and evaluate the effect of various process parameters on casting integrity.
- Apply developed technologies to the production of a selected automotive component.

Accomplishments

- Completed design of ASC machine.
- Reached 80% completion of fabrication of ASC machine.
- Designed and fabricated data acquisition system.
- Designed and fabricated gate shutoff mechanism.

- Designed and fabricated squeeze cast tooling.

Future Direction

- Complete fabrication of ASC machine and install data acquisition system.
 - Install ASC machine at Eck Industries.
 - Integrate operation of gate shutoff mechanism with the casting machine control system.
 - Develop and evaluate ASC process technologies.
 - Demonstrate production viability of ASC casting machine and process.
-

Introduction

Squeeze casting is the solidification of liquid metal under pressure in a closed metal die. The resulting casting has improved properties and a more uniform microstructure compared with those produced by traditional molten metal fabrication techniques. The higher properties are achieved through controlled entry of the metal into the die through large gates, which reduces turbulence, and high solidification rates, resulting in refinement of microstructural features.

There are two squeeze casting methods—direct and indirect. The method and efficiency of pressure application distinguish the two processes. Direct squeeze casting applies pressure directly on the casting. Indirect squeeze casting applies pressure via the gating system. The length of the gating system and any partial solidification prior to complete solidification of the part reduces the magnitude of the pressure applied and may result in casting porosity. For the indirect squeeze cast method, the dimensions of the die cavity control the part dimensions. For direct squeeze casting, the part dimensions are controlled by the die cavity dimensions and the finish position of the top die. Thus the direct squeeze cast method requires precise machine control to attain the desired part dimensions. In addition, the direct method requires in-gate shutoff technology to control pressure during cavity pressurization. Both methods suffer from poor metal handling from the furnace into the mold or gating system. Inadequate control of pouring speed generates turbulence and casting defects, such as oxide inclusions, that reduce fatigue properties.

Earlier attempts to improve the squeeze casting process by combining the advantages of low-

pressure die fill with those of squeeze casting demonstrated substantial mechanical property improvement and reduced component porosity. However, continuous production operation of the equipment was not achieved. The machines used were not specifically designed to meet the needs of the process.

Technical Approach

The results of this project will provide (1) a production-viable ASC machine, (2) process technology that will improve the strength and reliability of cast automotive components, and (3) demonstrated production viability of the equipment and process.

Machine Design. Previous efforts have demonstrated that modification of existing cast machine designs does not provide a production-capable ASC machine. An assessment of the capabilities and limitations of existing machine designs demonstrated that

- Low-pressure casting equipment typically does not have the structural rigidity needed to withstand the high pressures required of squeeze casting.
- Die-casting and currently available squeeze casting machines are not designed for proper (nonturbulent) molten metal entry into the die cavity.
- Neither type of equipment is typically available with the hydraulic and electronic controls necessary to attain the die cavity motions required for the direct squeeze casting process.

After much consideration, the project team decided it was easier and more cost-effective to build a machine from the ground up than to modify an existing cast machine design. To facilitate this design and construction, the team partnered with Empire Castings, Inc., an experienced producer of low-pressure casting equipment.

Process Development. Bendix, Inc. is an industrial manufacturer of truck components with an interest in reducing manufacturing cost by the use of high-quality castings. Consultation with Bendix led to the selection of an air compressor connecting rod for prototype production in the ASC machine. This component has a level of complexity that can demonstrate the production capability of the ASC machine and process and the need for mechanical properties higher than those attainable with commercially available castings, and it provides an opportunity for production with the ASC process.

The cast part will be modeled for fluid flow and solidification. This work will be done in parallel with equipment design. Simulation will provide an understanding of optimum metal flow conditions and squeeze requirements, if any, to contend with solidification shrinkage. This is very important to the success of the program and potentially to the details of the machine design. The ASC machine will have two mechanisms to feed the casting—low-pressure, nonturbulent fill of the die cavity and high-pressure, direct squeeze to minimize solidification shrinkage. Modeling experiments will explore the interaction of the two feed mechanisms and select process parameters that lead to process optimization. Modeling results will be used to refine the die design and select initial casting process parameters.

After tooling construction and ASC machine delivery, castings will be made under the range of process conditions anticipated during modeling. A variety of both cast and wrought alloys (Table 1) will be used. Evaluation of those castings will include radiography, die penetrant inspection, tensile testing, and functional component testing at Bendix. It is anticipated that this part of the program will require multiple iterations to produce the desired product quality. Some equipment and tooling modification may be required during this part of the program.

Table 1. Aluminum alloys to be used for casting trials

AA 380	AA 206
AA 356	AA 6061
AA 357	AA 535
AA 319	AA 388

After successful production of development castings, the production viability of the equipment and process will be demonstrated by

- Production of a connecting rod with reduced porosity and improved mechanical properties compared with the current die-cast connecting rod used by Bendix.
- Continuous production with the ASC machine and connecting rod tooling to include at least one 5-h continuous run with the equipment running at least 3 days in a week.

The goal of the project team is to implement part production on an ongoing basis. The production phase of the project will include detailed cost analysis of part production, determination of die-life parameters, and ongoing equipment and tooling development for maximum uptime.

Program Status

ASC machine. The design (Figure 1) for the 600-ton capacity ASC machine has been completed. Positioning of the top die is accomplished independently of the squeeze-cast cylinder. To maximize machine capability, the melting vessel is equipped with a crucible furnace. This facilitates the melting of both cast and wrought aluminum and magnesium alloys as well as aluminum and magnesium metal matrix composite alloys.

To match the dimensional capabilities of the die-cast process, a closely controlled volume of liquid metal must be fed into the die cavity. Conventional low-pressure fill technology does not have the capability to accurately meter a fixed amount of liquid metal into the die. Therefore, we will accurately position (± 0.13 mm) the top die to obtain the desired fill volume and use a fill sensor and an independently controlled gate shutoff to control metal volume. Development of a reliable gate shutoff technology is a key part of the ex-

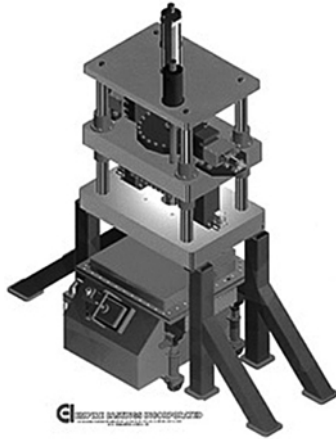


Figure 1. Design for 600-ton ASC machine.

perimental program. Gate shutoff system components are shown in Figure 2.

Data acquisition system. A computerized data acquisition system has been designed to interface with the displacement, pressure, and temperature sensors located on the ASC press and cast tooling. Analysis of these data will be critical in understanding the operation of the ASC process. This system will be installed on the machine in early November.

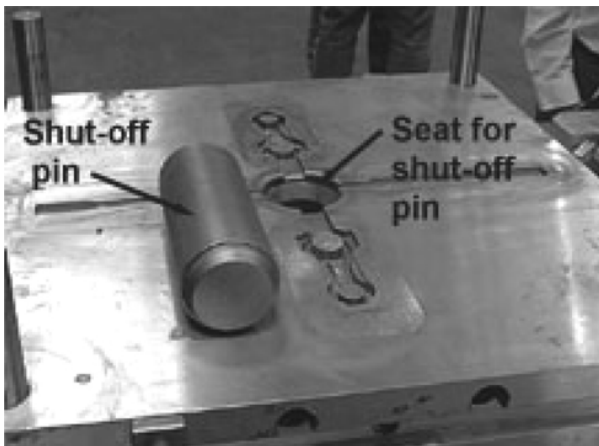


Figure 2. Components of the in-gate shutoff system.

Cast tooling. The die for casting air-compressor connecting rods and tensile test bars has been completed. As shown in Figure 3, the tooling consists of a die holder and individual die inserts for the particular part being cast. This tooling will be used for the machine run-off.



Figure 3. View of cast tooling.

Conclusions

Good progress has been made on the project. The steel shortage and prior commitments of the machine builder delayed press construction by about 6 months. This is reflected in the revised schedule (Table 2). All other tasks of the project are on schedule. The results of casting simulation should decrease the process development time required to the 3 months reflected in the revised schedule.

F. Thermomechanical Processing of Ti and Ti-6Al-4V Sheet and Plate

Principal Investigator: Craig A. Blue

Oak Ridge National Laboratory

Oak Ridge, TN 37831-8063

(865) 574-4351; fax (865) 574-4357; e-mail: blueca@ornl.gov

Field Project Manager: John D. K. Rivard

Oak Ridge National Laboratory

Oak Ridge, TN 37831-8063

(865) 241-8113; fax (865) 574-4357; e-mail: rivardjd@ornl.gov

Technology Development Area Specialist: Sidney Diamond

(202) 586-8032; fax: (202) 586-1600; e-mail: sid.diamond@ee.doe.gov

Field Technical Manager: Philip S. Sklad

(865) 574-5069; fax: (865) 576-4963; e-mail: skladps@ornl.gov

Participants

Evan K. Ohriner, Oak Ridge National Laboratory

David C. Harper, Oak Ridge National Laboratory

Jim O. Kiggins, Oak Ridge National Laboratory

Paul A. Menchhofer, Oak Ridge National Laboratory

Lance Jacobsen, International Titanium Powder, L.L.C.

Dariusz Kogut, International Titanium Powder, L.L.C.

Contractor: Oak Ridge National Laboratory

Contract No.: DE-AC05-00OR22725

Objective

- Investigate and develop vacuum hot pressing (VHP) methods for the production of titanium (Ti) and Ti-6Al-4V plate from Ti and Ti-6Al-4V powder provided by International Titanium Powder, LLC (ITP).
- Simulate a roll compaction method for the manufacturing of Ti and Ti-6Al-4V thin-gage sheet from Ti and Ti-6Al-4V powder provided by ITP.
- Demonstrate the ability to process thin-gage sheet using powder Ti precursor and plasma arc lamp processing.
- Mechanically test Oak Ridge National Laboratory (ORNL)-produced materials
- Optically and chemically analyze ORNL-produced materials.

Approach

- Conduct parametric studies using VHP to consolidate ITP Ti and Ti-6Al-4V powder to demonstrate the feasibility of powder use for further experiments.
- Develop roll compaction techniques for the production of thin-gage Ti and Ti-6Al-4V from ITP powder using infrared (IR) heating from tungsten halogen lamp furnaces and plasma arc lamp.

- Characterize ORNL-produced material properties.
- Develop approach to scaling processing techniques for large-scale production applications.

Accomplishments

- Successfully consolidated ITP Ti and Ti-6Al-4V powder using VHP.
- Developed processing techniques for production of thin-gage sheet using IR heating.
- Evaluated physical, microstructural, and chemical properties of ORNL-produced materials

Future Direction

- Partner with ITP and Ametek to scale process to produce Ti and Ti-6Al-4V sheet and plate at substantially reduced cost using a lab-scale roll compaction process as a basis for commercial processing.
- Partner with Universal Alloy Cooperation to extrude ITP Ti and Ti-6Al-4V rod and plate. Plates up to 40 in. wide can be extruded.

Introduction

The aircraft industry is currently the single largest market for Ti and Ti alloy products primarily because of the exceptional strength-to-weight ratio, elevated temperature performance, and corrosion resistance.

Titanium usage, however, is strongly limited outside the aerospace industry by its higher cost relative to competing materials, primarily aluminum alloys and steels. Although Ti possesses an attractive set of properties, including high specific strength and corrosion resistance, and allows for damage-tolerant design, cost limits applications to selected markets. Many automotive systems would benefit from the use of Ti products. Automotive exhaust systems could save as much as 50% of their current weight by integrating Ti parts. Titanium valves and valve springs, connecting rods, suspension springs, wheels, drive shafts, underbody panels, side impact bars, and half shafts are just some of the automotive applications that could benefit from the use of Ti.

The present market comparison for the use of engineering materials shows that steel is the most widely used material, with 800 million tons used each year. Aluminum, stainless steel, and copper are used at a rate of 22 million tons, 16 million tons, and 12 million tons, respectively. Titanium is much less widely used at 0.05 millions tons per year.

Potential technical problems preventing the integration of Ti, apart from cost of manufacturing, include wear resistance, a lower modulus than steel, and machining difficulties. Wear resistance can be

addressed by coatings/reinforcements; the modulus can be increased by reinforcing the part with a second material; and the machining difficulties can be reduced by the production of near-net-shape parts. The major problem is that Ti costs substantially more than competing materials.

Although the cost of Ti ore is significantly more than that of other competing materials, the difference in the cost of sheet is a result of processing. Processing of Ti from ingot to plate accounts for 47% of the total cost of the material.

Current melting techniques include vacuum arc remelting (VAR), electron beam melting, and plasma arc single-melt processes. VAR is used to clean and refine air-melted ingots and to improve homogeneity and refine grain size. To VAR-cast an ingot, a dc arc is struck between a Ti electrode and a base plate. The intense heat melts the electrode, and the Ti is cast into an ingot. VAR requires 20 hours and large-scale equipment.

Electron beam and plasma arc single-melt processes have the advantage over VAR in that an air-melted ingot is not required. In these two processes, ingots are cast directly from melted feed sponge. But the cast ingot still requires post-processing, which accounts for 47% of the total cost. The plasma arc melt process is similar; plasma arc torches are used in place of electron beams for melting.

Alternative processing methods such as casting, laser forming, and spray forming have also been explored. Casting is best suited for complex shape forming and is not economical for sheet processing. The process requires extensive tooling and frequent

inspections. A post-hot isostatic pressing (HIP) is needed to eliminate porosity. Laser forming uses a raw powder stream injected into a rastered laser beam to melt, form, and build up sheet. Spray forming operates similarly, although a plasma torch melts the powder. Laser forming and spray forming have the advantages of using less material, requiring minimal tooling, and needing short cycle times. But it is difficult to control the thermal history of laser forming, and both methods suffer from residual porosity. In addition, both of these methods require conventionally produced and atomized powder, which is very costly.

Although much time and effort has been invested in the development of these processing techniques, the cost of Ti still remains high because of the cost of raw materials, cost of post-processing, and yield losses. In recent work performed at the Infrared Processing Center at ORNL, new methods of Ti sheet and plate processing have been investigated. VHP, high-density infrared (HDI) processing, and roll compaction processing were explored. All three methods used powder provided by ITP. ITP has developed a new low-cost method of powder production and is currently running a pilot processing facility.

Experimental Procedure

ITP Ti powder was processed into plate and sheet using three methods, VHP, HDI, and roll compaction. ITP Ti-6Al-4V was processed into plate and sheet using VHP and roll compaction. VHP, a batch process, was used to make Ti and Ti-6Al-4V plate. HDI and roll compaction were both used to make Ti sheet. Roll compaction also was used to make Ti-6Al-4V sheet. HDI uses a plasma arc lamp to heat and liquid-phase-sinter vacuum-cold-pressed Armstrong Process Ti powder. Sintered compacts were repeatedly cold-rolled and flash-annealed under the plasma arc lamp in order to make sheet. Similarly, roll compaction uses medium-density tungsten-halogen-based radiant heating to solid-phase-sinter vacuum-cold-pressed Armstrong Process Ti and Ti-6Al-4V powder. Sintered compacts were repeatedly cold-rolled and annealed until thin-gage sheet was produced.

VHP was used to make four samples of Ti plate and one Ti-6Al-4V plate. Each of the four samples was pressed under vacuum in a graphite element radiant furnace. The three Ti samples and the Ti-

6Al-4V sample were pressed in a 63.5-mm-diam graphite die. The fourth sample was pressed in a 178-mm-diam die. For each of the pressing operations, the die was lined with Grafoil and a measured amount of Ti powder was poured into the die. For the 63.5-mm-diam samples, the die was filled with 36 g of Ti or Ti-6Al-4V powder. And for the 178-mm-diam sample, the die was filled with 130 g of Ti powder. To prevent mechanical interaction between air and the powder, no pre-pressing was applied. A special collar was placed under the die to keep it in place while the powder was being pressed. When the rams were jogged into place, the furnace was closed, sealed, and evacuated. The furnace was back-filled with argon gas and evacuated three times in order to ensure a clean processing environment. The 63.5-mm-diam Ti samples were pressed at a pressure of 55.3 MPa. One sample was pressed at 750°C for 15 min, another sample was pressed at 900°C for 15 min, and the final sample was pressed at 900°C for 30 min. The Ti-6Al-4V 63.5-mm-diam sample was pressed at a pressure of 55.3 MPa for 1 hour at 950°C. The 178-mm-diam Ti sample was pressed at a pressure of 11.7 MPa for 1 hour at 900°C. All five samples were allowed to furnace cool after the heating cycle was completed. After the samples were removed from the furnace, the sample surfaces were ground and polished, and the densities were measured by immersion in ethanol (Archimedes method). Tensile specimens were machined from each 63.5-mm-diam sample. The tensile specimens were machined to the SS3 standard. Mechanical testing, chemical analysis, and optical microscopy were performed on the samples.

Roll compaction was developed by Ametek Corporation for the commercial production of nickel and other advanced alloy sheet. With ITP Ti powder costing as little as \$4/lb, and with the greatly reduced effort needed to obtain sheet compared with the ingot processes, roll compaction could eliminate a large portion of total Ti sheet fabrication costs dedicated to forming. Roll compaction begins with raw powder fed into rolls from a hopper. The rolls compact the ductile powder into sheet. The sheet is then fed into a furnace where the sheet is sintered. Subsequent roll and sinter operations are performed continuously until a dense, thin-gage sheet is produced.

To simulate a roll compaction process on a laboratory scale, thin-gage sheet was produced by sinter-

ing powder compacts in an IR furnace followed by cold rolling. First, 18 g of Ti or Ti-6Al-4V powder was vacuum-cold-pressed in a 50.8-mm-diam die at a pressure of 48.3 MPa. Powder compacts were heated in a 33-kW IR furnace that contains a 152-mm-inside-diam quartz tube that allows for vacuum and argon gas flow in the chamber.

The Ti sample was heated to 1200°C, held for 2 hours, and then furnace-cooled and cold-rolled. The initial thickness was 3.25 mm; after rolling, it was 1.29 mm. The sample was again heated at 1200°C for 2 hours in the IR furnace. The sample was then cold-rolled from 1.29 to 0.53 mm. A final anneal of 1200°C for 1 hour was then performed on the sample.

The Ti-6Al-4V sample was heated to 950°C and held for 2 hours and then furnace-cooled and cold-rolled. The initial thickness was 4.06 mm, and thickness after rolling was 1.90 mm. The sample was again heated at 950°C for 30 min in the IR furnace. The sample was then cold-rolled from 1.90 to 0.97 mm. Another intermediate anneal was performed by heating the sample to 950°C for 30 min. A final cold-roll was performed, and the final gage thickness was measured at 0.61 mm. A final 950°C/30-min stress relief was also performed.

From each final sheet, tensile specimens were machined and tested, chemical analysis was performed, and the microstructure was investigated.

HDI processing is similar to roll compaction but uses heating the sample to the liquid phase to achieve bonding. In order to achieve temperatures above the 1650°C melting point of Ti, a plasma arc lamp is used to rapidly heat a vacuum-cold-pressed compact. The plasma arc lamps use a unique technology to produce extremely high power densities with a single lamp. Instead of an electrically heated resistive element, controlled and contained plasma is used.

The lamp is sealed at the ends where the cathode and anode are located. Deionized water mixed with argon gas enters at the cathode side through high-velocity jets impinging at a given angle. Because of the high velocities and pressure, the deionized water is impelled to the wall of the quartz tube and spirals down the length of the tube in a uniform 2- to 3-mm-thick film. This water film serves two purposes: to cool the quartz wall and to remove any tungsten particulates that may be expelled from the electrodes. The gas moves in a spiral fashion through the

center of the tube, and a capacitive circuit initiates the plasma. The lamp operates at 750,000 W and is fitted with a reflector that illuminates a 20×15 cm area with a power density of up to 460 W/cm². The plasma, which has a temperature in excess of 10,000 K, is stable and produces a radiant spectrum from 0.2 to 1.4 μm.

The processing steps for HDI were very similar to those for roll compaction. First, 9 g of raw Ti powder was vacuum-cold-pressed in a 50.8-mm-diam steel die under 48.3 MPa pressure. The cold-pressed compact was then placed in an environmentally controlled processing box. The box was water cooled and vacuum-tight. The box was evacuated and back-filled with argon gas to reduce oxidation during processing.

The sample was moved into position under the lamp and liquid-phase-sintered at 280 W/cm² for 8.5 s. The thickness after sintering was measured at 1.8 mm. After a cold-rolling operation, the sample measured 0.95 mm. The cold-rolled sample was flash-annealed under the lamp at 280 W/cm² for 5 s. The sample was then rolled to 0.62 mm. A second flash anneal was performed at 280 W/cm² for 5 s. A final cold roll was performed, and the final thickness measured 0.40 mm. The sample was flash-annealed at 100 W/cm² for 5 s. The thin-gage, annealed sheet was mechanically tested, chemically analyzed, and observed under a light microscope.

Results and Discussion

After the post-pressing grinding and machining was performed on the VHP Ti and Ti-6Al-4V consolidated powder, the samples were polished. Figure 1 shows the final Ti plates.

The density of each plate was measured by the Archimedes method to be 100%. But metallographic observations performed on a light microscope showed differences in the levels of sintering obtained for the three pressing conditions. Figure 2 shows the microstructure of the VHP samples

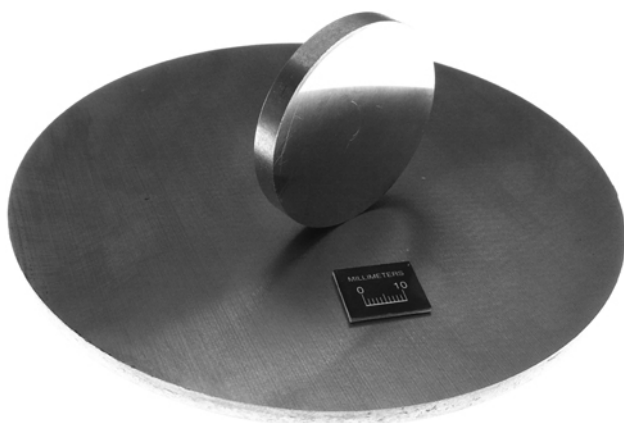


Figure 1. As-VHP and machined Ti plates, 63.5 mm diameter and 178 mm diameter.

at 750°C for 15 min, 900°C for 15 min, and 900°C for 30 min.

Figure 2a shows that sintering in the 750°C/15 min samples was incomplete, and many voids in the microstructure still remained. Figure 2b shows that increasing the pressing temperature to 900°C helps to reduce the amount of void present. But the best results were obtained by pressing at 900°C for 30 min. Figure 2c shows the least amount of void after pressing at 900°C for 30 min and shows that grain growth has occurred, indicating that the particles have fully bonded to each other. Figure 2d shows the microstructure of the VHP Ti-6Al-4V samples.

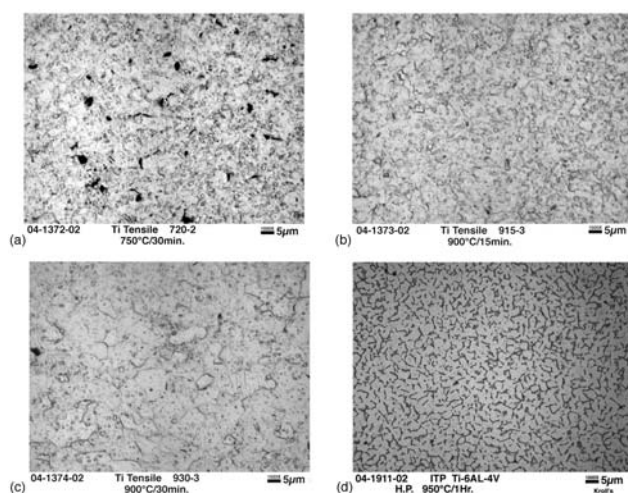


Figure 2. Microstructure for VHP samples (a) Ti 750°C/15 min, (b) Ti 900°C/15 min, (c) Ti 900°C/30 min, and (d) Ti-6Al-4V 950°C/1h4.

The lack of sintering at 750°C and 900°C/15 min was also apparent in mechanical testing. Each of

the SS3 tensile specimens machined from the 63.5-mm-diam plates was tested in tension with a cross-head speed of 0.51 mm/min. The mechanical testing results are shown in Table 1.

According to Allegheny Ludlum, Grade 2 Ti has comparable properties to the 930°C/30 min VHP samples. The Ti-6Al-4V VHP samples also exceeded the properties published for this material. Chemical analysis showed that the VHP Ti samples were all below the maximum allowable limits of O₂, N₂, and C for Grade 2 Ti. The O₂ content of the VHP Ti-6Al-4V slightly exceeded the upper limits for Grade 5 Ti-6Al-4V, but the high oxygen level did not adversely affect mechanical testing results. The results of the chemical analysis are shown in Table 2.

Microstructural investigations were performed on the HDI-processed roll-compacted Ti and on roll-compacted Ti-6Al-4V thin-gage sheet materials. Both samples were cut from the as-annealed sheet, mounted, polished, and etched with Kroll's reagent. Optical microscopy revealed that the roll-compacted sample had a standard annealed Ti microstructure. Throughout the entire cross section, the roll-compacted sheet was virtually free of flaws with a very consistent microstructure. The HDI-processed material showed that the intense, short-duration, and directional heating of the plasma arc lamp caused large grains to grow on the top surface during the final anneal. But the structure remained equiaxed alpha with beta spheroids. Also, microscopy showed that many rolling lapses remained in the final HDI-processed sheet. Investigation of the structure of the roll-compacted Ti-6Al-4V sheet showed that a significant amount of retained oxygen-stabilized-α was present. Figure 3 shows the microstructure of the HDI-processed Ti sheet, the roll-compacted Ti sheet, and the roll-compacted Ti-6Al-4V sheet.

Mechanical testing of the HDI-processed and roll-compacted sheet was performed. Tensile testing results are shown in Table 3.

The lack of ductility of the HDI-processed samples was due to the observed rolling lapses. This is similar to the lack of complete sintering in the 750°C/15 min VHP sample. The mechanical properties of roll-compacted Ti sheet showed that the strengths are comparable to Grade 4 Ti. But the oxygen content of the roll-compacted samples exceeded the allowable limit for Grade 4, and the ductility suffered as a result. The chemical analysis

Table 1. Mechanical testing results of VHP Ti and Ti-6Al-4V plates

Sample	Yield strength [MPa]	Tensile strength [MPa]	Elongation [%]
Ti 750°C/15min	532	571	1.7
Ti 915°C/15min	544	636	14.9
Ti 930°C/30min	517	617	20.7
Ti grade 2 (min values)	345	448	20.0
Ti-6Al-4V 950°C/1 hour	963	994	13.8
Ti-6Al-4V grade 5 (min values)	828	897	10.0

Table 2. Chemical analysis of VHP Ti and Ti-6Al-4V plate (nominal %)

Sample	O ₂ [%]	N ₂ [%]	C [%]
Ti 750°C/15min	0.23	0.01	0.05
Ti 900°C/15min	0.25	0.01	0.06
Ti 900°C/30min	0.24	0.01	0.03
Ti grade 2 (max limits)	0.25	0.03	0.08
Ti-6Al-4V 950°C/1hour	0.28	0.01	0.04
Ti-6Al-4V grade 5 (max limits)	0.20	0.05	0.08

Table 3. Mechanical testing results of HDI-processed and roll compacted Ti sheet

Sample	Yield strength [MPa]	Tensile strength [MPa]	Elongation [%]
HDI-processed Ti	486	598	8.8
Roll-compacted Ti	529	656	9.6
Ti grade 4	483	552	15.0

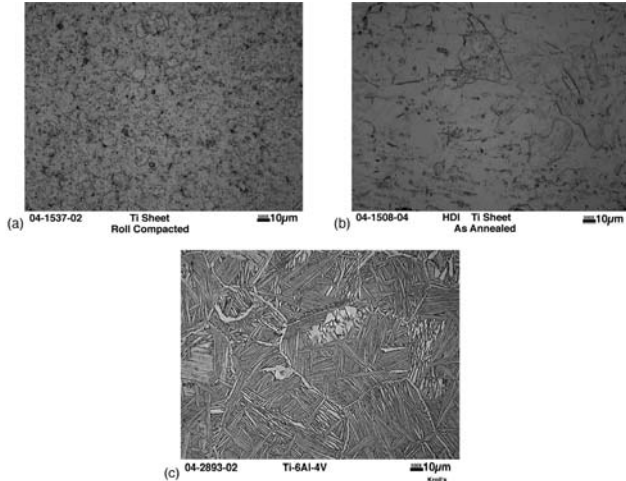


Figure 3. Microstructure for thin-gage sheet samples (a) roll-compacted Ti, (b) HDI-processed Ti, and (c) roll-compacted Ti-6Al-4V.

of the HDI-processed and roll-compacted material is shown in Table 4.

Summary

These are the highlights of the progress during FY 2004:

1. Production of VHP Ti plate with mechanical properties comparable to those of commercially pure Ti grade 2.
2. Production of VHP Ti-6Al-4V plate.
3. Roll compaction of Ti and Ti-6Al-4V thin-gage sheet.
4. Production of HDI-processed Ti thin-gage sheet.
5. Mechanical, optical, and chemical analysis of ORNL-produced sheet.

Conclusions

Although Ti and Ti-6Al-4V have attractive properties that would benefit a great number of engineering applications, their use is limited by the cost of the raw material and the processing that is necessary to make a usable product. But with the recent advancements in low-cost powder production at ITP, in conjunction with processing techniques

Table 4. Chemical analysis of HDI-processed and roll compacted thin gage Ti sheet

Sample	O ₂	N ₂	C
HDI-processed Ti	0.29	0.01	0.03
Roll-compacted Ti	0.42	0.01	0.03
Ti grade 4 (max limits)	0.40	0.05	0.08

developed at ORNL, the cost of Ti sheet and plate is predicted to decrease. While VHP on a large scale may not be an economical method of plate production, it does demonstrate that ITP powder can produce a viable product. HDI-processing could be developed into a commercial process, but liquid-phase processing may not be desirable. Furthermore, HDI-processed Ti sheet lacks the mechanical properties necessary. Roll compaction is the best alternative to the current VAR and other ingot metallurgy

processes used to process Ti. Processing facilities are in place to produce nickel alloys and could easily be modified to process Ti. Lab-scale roll compaction produced thin-gage Ti sheet with the appropriate microstructure, mechanical properties, and chemical composition. Although the ductility is slightly below acceptable levels, a scaled-up facility will have better control over oxygen contamination, eliminating this problem. Results suggest that the roll compaction of Ti sheet should be further explored.

